

Direct numerical simulations of the effects of shear on turbulent Rayleigh–Bénard convection

By J. ANDRZEJ DOMARADZKI†
AND RALPH W. METCALFE‡

† Department of Aerospace Engineering, University of Southern California,
Los Angeles, CA 90089-1191, USA

‡ Department of Mechanical Engineering, University of Houston,
Houston, TX 77004, USA

(Received 24 February 1987 and in revised form 1 February 1988)

The interaction between shear and buoyancy effects for Bénard convection in plane Couette flow is studied by performing direct numerical simulations. At moderate Rayleigh numbers (≈ 10000 – 50000), shear tends to organize the flow into quasi-two-dimensional rolls parallel to the mean flow and can enhance heat transfer, while at higher Rayleigh numbers (> 150000), shear tends to disrupt the formation of convective plumes and can reduce heat transfer. A significant temporal oscillation in the local Nusselt number was consistently observed at high Rayleigh numbers, a factor that may contribute to the scatter seen in experimental data. This effect, plus the time-varying reversal of the mean temperature gradient in the middle of the channel, is consistent with a flow model in which the dynamics of large-scale, quasi-two-dimensional, counter-rotating vortical cells are alternately driven by buoyancy and inertial effects. An analysis of the energy balance in the flow shows that the conservative pressure diffusion term, which has been frequently neglected in turbulence models, plays a very important dynamical role in the flow evolution and should be more carefully modelled. Most of the turbulent energy production due to mean shear is generated in the boundary layers, while the buoyant production occurs mainly in the relatively uniform convective core. The simulations and the laboratory experiments of Deardorff & Willis (1967) are in very reasonable qualitative agreement, suggesting that the basic dynamics of the flow are being accurately simulated.

1. Introduction

Laminar and turbulent Bénard convection has been the subject of intensive theoretical, experimental, and numerical study in recent years. However, in many important engineering and geophysical flows, thermal convection occurs in the presence of mean shear. For example, in heat exchangers, one fluid is often pumped through pipes or channels to enhance the heat transfer with the other fluid. The resulting flow is a complex interaction between buoyancy-driven and shear effects. The presence of background shear can very dramatically alter the dynamics of the flow, so a better understanding of these effects is essential for the development of better techniques for simulating and modelling such flows. The interaction between convection and shear is also very important in geophysical flows in the atmospheric and oceanic boundary layers.

There are two useful dimensionless quantities for characterizing convective shear flows. First is the Richardson number:

$$Ri = |\mathbf{g}| \alpha \frac{\partial \bar{T} / \partial z}{(\partial \bar{U} / \partial z)^2}, \quad (1)$$

where \mathbf{g} is the gravitational acceleration, α is the coefficient of thermal expansion, $\bar{T}(z)$ and $\bar{U}(z)$ are the mean temperature and velocity respectively, and z is directed upwards, opposite to \mathbf{g} . The other convenient parameter is the Monin–Obukhov length:

$$L = - \frac{u_*^3}{|\mathbf{g}| \alpha \tilde{\kappa} \frac{q}{c_p \rho_0}}, \quad (2)$$

where u_* is the friction velocity (Monin & Yaglom 1979), q is the vertical heat flux, c_p is the specific heat at constant pressure, ρ_0 is a reference density of the fluid and $\tilde{\kappa}$ is the von Kármán constant. For unstable conditions, both Ri and L are negative. Most research on unstable convective shear flows has focused on two limiting cases: $Ri \rightarrow -\infty$ (or $z/L \rightarrow -\infty$), and $Ri \rightarrow 0_-$ (or $z/L \rightarrow 0$), where 0_- indicates that zero is approached through negative values. In the first case, buoyancy forces dominate, while in the latter, shear effects are most important, so that the temperature-field acts as a passive scalar.

Free convection has been extensively studied for Bénard convection in a layer of fluid between two horizontal, parallel plates heated from below. In this case, the important non-dimensional parameters are the Prandtl number:

$$Pr = \nu / \kappa, \quad (3)$$

where ν is the kinematic viscosity and κ is the thermal diffusivity, and the Rayleigh number:

$$Ra = (|\mathbf{g}| \alpha / \kappa \nu) \Delta T d^3, \quad (4)$$

where ΔT is the temperature difference between the plates separated by a distance d . Early work on the stability of the Bénard problem is discussed by Chandrasekhar (1961). The experimental work of Malkus (1954), Deardorff & Willis (1967), Krishnamurti (1970*a, b*, 1973) and Brown (1973) revealed a number of discrete heat-flux transitions with increasing Rayleigh number. In addition, Krishnamurti (1973) documented experimentally the existence of different flow regimes in the (Ra, Pr) -plane with the complexity of the flow field increasing from quiescent to fully turbulent with increasing Rayleigh number. This increased complexity is manifested by the appearance of temporal oscillations of the velocity and temperature fields as documented by Deardorff & Willis (1967), Willis & Deardorff (1965, 1970), Rossby (1969) and Krishnamurti (1970*a, b*). In addition, the spatial power spectrum of the temperature field broadens (Willis & Deardorff 1965). The experiments of Deardorff & Willis (1967), Goldstein & Chu (1969), and Chu & Goldstein (1973) provide important data on Bénard convection for high Rayleigh numbers in the turbulent regime.

Theoretical work has concentrated on stability analysis, predicting as the only stable flow parallel convective rolls for slightly supercritical Rayleigh numbers in an infinite layer between two rigid plates (Schlüter, Lortz & Busse 1965). Transition to time-dependent Bénard convection was investigated by Busse (1972) and Clever & Busse (1974). Classical experimental work and stability analysis do not provide

detailed quantitative information about the full velocity and temperature fields under these conditions. They are generally concerned with the global properties of the convection, such as heat transfer, transitions between different flow regimes, the structure of the convective cells, etc. Detailed measurements of the velocity field at one point in Bénard cells are possible using LDV techniques as demonstrated by Bergé & Dubois (1976), Dubois & Bergé (1978), Ahlers & Behringer (1978), and Gollub *et al.* (1977). Still more detailed information about the entire velocity and temperature fields may be obtained from the accurate numerical solutions of the equations governing natural convection. This approach was used by Lipps (1976) to investigate thermal convection in air for Rayleigh numbers between 4000 and 25000. Numerical methods were used by McLaughlin & Orszag (1982) and Curry *et al.* (1984) to investigate transition to chaos in Bénard convection. Direct numerical simulations of turbulent convection can encounter resolution problems, as discussed by Grötzbach (1983). Since this serves to limit the Rayleigh number of the flow that can be accurately simulated, the largest Rayleigh-number simulations reported so far in the literature are for $Ra = 380000$ (Grötzbach 1982; Eidson, Hussaini & Zang 1986). Convection with higher Rayleigh numbers was numerically simulated by Daly (1974) using a turbulence model and by Eidson (1985) using subgrid-scale modelling.

In the case of forced convection ($Ri \rightarrow 0_-, z/L \rightarrow 0_-$) for moderate Prandtl numbers, the Reynolds analogy between momentum and heat transfer in turbulent flows, which states that the turbulent Prandtl number is constant and close to unity, can be used. The Reynolds analogy and departures from it in the wall region are discussed by Hinze (1975) and in the geophysical context by Monin & Yaglom (1979).

The regions of free and forced convection are separated by a region where the effects of shear and convection may be equally important. The effects of moderate shear on thermal convection were investigated by Hart (1971) and Sparrow & Husar (1969), who performed experiments on an inclined heated plate. In his experiments, Ingersoll (1966) used a cylindrical container with a heated lower wall and the upper wall rotating about a vertical axis. The experiments of Richter & Parsons (1975) were performed in a large-aspect-ratio square container with a heated lower wall and an upper boundary moving horizontally. The main qualitative conclusion from these experiments is that the presence of the vertical shear organizes convective rolls in the direction of the mean velocity and suppresses rolls in the direction transverse to the mean flow. The stability analysis of Kuo (1963) and the two-dimensional numerical simulations of Lipps (1971) are consistent with these experimental results. Clever & Busse (1977) and Clever, Busse & Kelly (1977) investigated theoretically transition from purely two-dimensional steady convection rolls to three-dimensional convection in the presence of vertical shear. The only numerical investigation of three-dimensional convection in plane Couette flow with heated boundaries known to the present authors has been reported recently by Hathaway & Somerville (1986).

The most important quantitative global effect of the mean shear is a modification of the heat transfer. There is a controversy in the literature as to the direction of change in the heat transfer when a mean flow is present. For example, Hathaway & Somerville (1986) reported that, for small shear, the heat flux is lower than for the unsheared case and the same Rayleigh number. However, they found that when the shear becomes larger, the heat flux also increases. Similarly, the two-dimensional numerical results of Lipps (1971) for convection with shear for $Pr = 0.7$ and Ra in the range 10000 to 40000 give a consistently greater heat flux than corresponding results

of Clever & Busse (1974) for unsheared cases. On the other hand, the experiments of Ingersoll (1966) indicate a lower heat flux in the presence of shear. For atmospheric boundary-layer flows, the non-dimensional heat flux is practically unaffected by shear even for low Richardson numbers of around -0.02 . For still higher values of shear with Richardson numbers above -0.02 , the heat flux is increased by the presence of shear (Monin & Yaglom 1979, figures 51 and 67). Such diverse results certainly suggest that the interaction between heat transfer and mean shear involves some rather complex dynamical processes. Moreover, the accurate experimental and numerical data on three-dimensional convection with shear are rather scarce, especially in the range of Rayleigh and Richardson numbers in which the effects of shear and buoyancy are comparable.

The objectives of this work are to perform accurate numerical simulations of turbulent convection with mean shear in order to address some of these questions and to enhance our understanding of such flows. As a model problem we have chosen plane Couette flow with a heated lower boundary. Though some of the results were obtained for low Rayleigh numbers, we were generally interested in the range of Rayleigh numbers above 30000 where the Bénard convection in air without shear is known to be turbulent. We have investigated the time dependence of temperature, velocity and heat flux in our runs, since this information is usually difficult to obtain experimentally but is easily available in the numerical simulations. An analysis of the kinetic-energy-balance and thermal-variance equations provides insight into the dynamics of the flow field, and provides useful information about the behaviour of terms important in turbulence modelling. As a by-product of this investigation we have established some useful criteria for determining spatial and temporal resolution requirements for accurate simulations at given Rayleigh and Richardson numbers.

2. Equations of motion

The physical problem of convection in plane Couette flow (figure 1) is described by the following standard set of hydrodynamic equations with the Boussinesq–Oberbeck approximation:

$$\partial_t \mathbf{u} = \mathbf{u} \times \boldsymbol{\omega} - \alpha \tilde{T} \mathbf{g} - \nabla \pi + \nu \nabla^2 \mathbf{u}, \quad (5a)$$

$$\partial_t T = -\nabla \cdot (\mathbf{u} T) + \kappa \nabla^2 T, \quad (5b)$$

$$\nabla \cdot \mathbf{u} = 0, \quad (5c)$$

where $\mathbf{u}(x, y, z, t) = (u, v, w)$ is the velocity field, $T(x, y, z, t)$ is the temperature field, and \tilde{T} is the departure from the linear profile defined below. The mean velocity $U(z)$ with non-vanishing vertical shear $\partial U(z)/\partial z$ is directed along the x -axis. The Navier–Stokes equations (5a) are written in the velocity–vorticity formulation with the vorticity $\boldsymbol{\omega} = \nabla \times \mathbf{u}$ and the pressure head $\pi = (1/\rho_0)p + \frac{1}{2}|\mathbf{u}|^2$, where p is the pressure and ρ_0 is the reference fluid density. In the above equations ν is the kinematic viscosity, κ is the coefficient of the thermometric conductivity, α is the coefficient of thermal expansion and \mathbf{g} is the gravitational acceleration.

In our simulations, it is assumed that fluid is contained between two rigid plates separated by the distance d . There is a constant positive temperature difference ΔT between the lower and upper plates. The plates move with uniform velocity $\frac{1}{2}\Delta U$ in opposite directions in horizontal planes so that the velocity difference between the plates is ΔU . For numerical convenience, the components of the velocity and

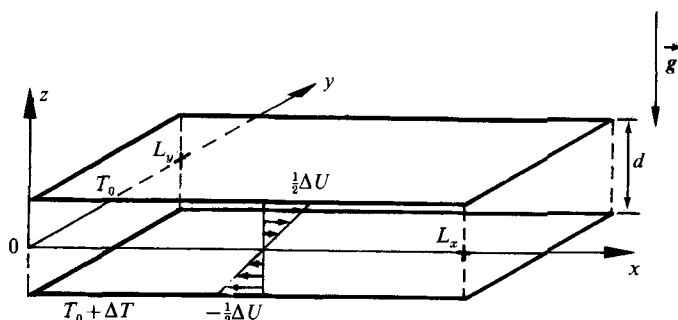


FIGURE 1. A schematic diagram of plane Couette flow with heated boundaries.

temperature fields contributing to the mean linear vertical gradients are factored out:

$$\mathbf{u}(x, y, z, t) = \frac{\Delta U}{d} z + \tilde{u}(x, y, z, t),$$

$$T(x, y, z, t) = T_0 - \frac{\Delta T}{d} (z - \frac{1}{2}d) + \tilde{T}(x, y, z, t).$$

It is assumed that $z \in [-\frac{1}{2}d, +\frac{1}{2}d]$ and $U(-\frac{1}{2}d) = -\frac{1}{2}\Delta U$, $U(\frac{1}{2}d) = \frac{1}{2}\Delta U$, $T(-\frac{1}{2}d) = T_0 + \Delta T$, and $T(\frac{1}{2}d) = T_0$, so that the boundary conditions for \tilde{u} and \tilde{T} are

$$\tilde{u}(x, y, \pm \frac{1}{2}d) = 0, \quad \tilde{T}(x, y, \pm \frac{1}{2}d) = 0. \quad (6a, b)$$

For numerical convenience, we employ periodic boundary conditions in the horizontal directions:

$$\tilde{u}(x + L_x, y + L_y, z) = \tilde{u}(x, y, z), \quad \tilde{T}(x + L_x, y + L_y, z) = \tilde{T}(x, y, z), \quad (6c, d)$$

where L_x, L_y are the periodicity lengths. Note that while this facilitates the computation of statistical quantities over horizontal planes of homogeneity, it does impose a limit on the largest scale of the spatial features that can be generated in the simulation. Non-dimensional parameters governing convection with shear are the Rayleigh number $Ra = |g|\alpha \Delta T d^3 / (\kappa \nu)$, the Prandtl number $Pr = \nu / \kappa$ and the Richardson number $Ri = g\alpha d \Delta T / \Delta U^2$. While equations (5) are commonly non-dimensionalized to make their dependence on Ra , Pr and Ri explicit, in our work we have used the dimensional form with values of the fluid properties in c.g.s. units corresponding to air, e.g. $Pr = 0.71$.

The numerical simulations provide values of velocity and temperature on all mesh points at each time step. These values are then used to compute other important quantities: the mean temperature $\langle T \rangle$ and mean velocity $\langle \mathbf{u} \rangle$ (the brackets $\langle \dots \rangle$ denote averaging over horizontal planes); and the normalized heat flux Nu (Nusselt number) and normalized momentum flux Mo in the vertical direction:

$$Nu = \frac{\langle w'T' \rangle - \kappa \partial_z \langle T \rangle}{\kappa \Delta T / d}, \quad Mo = \frac{\langle u'w' \rangle - \nu \partial_z \langle u \rangle}{-\nu \Delta U / d}. \quad (7a, b)$$

Here, and in subsequent formulae, primed quantities denote departures from the means $\langle \mathbf{u} \rangle$ and $\langle T \rangle$, which are sums of linear profiles, and $\langle \tilde{u} \rangle$ and $\langle \tilde{T} \rangle$, respectively.

Experiments of Deardorff & Willis (1967) provide information about the behaviour of the individual terms in the kinetic-energy and the thermal-variance equations, and we have also computed these terms in our numerical simulations. The derivation of these equations is formally the same as for turbulent flows (Monin & Yaglom 1979, p. 373) with the time averaging replaced by averaging over horizontal planes.

The kinetic-energy-balance equation can be written:

$$\begin{aligned}
 \frac{1}{2}\partial_t\langle q^2 \rangle &= -\langle u'_i u'_k \rangle \partial_k \langle u_i \rangle & E_{uw} \\
 &+ \alpha g \langle T' w' \rangle & E_{Tw} \\
 &+ \nu \langle (\partial_j u'_j + \partial_j u'_i) \partial_i u'_j \rangle & E_{DISS} & \text{Production} \\
 &-\hat{\partial}_k \langle p u'_k \rangle & E_{pw} \\
 &-\frac{1}{2}\hat{\partial}_k \langle q^2 u'_k \rangle & E_{www} \\
 &+ \nu \hat{\partial}_i \langle u'_j (\partial_j u'_i + \partial_j u'_j) \rangle & E_{NU} & \text{Diffusion,}
 \end{aligned} \tag{8}$$

where we use subscript notation $u_i = (u, v, w)$, $\partial_i \equiv \partial/\partial x_i$, and the summation convention is assumed. Here, $\frac{1}{2}q^2 = \frac{1}{2}(u'^2 + v'^2 + w'^2)$. All terms in (8) are non-dimensionalized by κ^3/d^4 . The terms E_{uw} and E_{Tw} describe the process of energy production by the shear and the buoyancy, respectively. The effect of viscous dissipation is described by the terms E_{DISS} . Finally, the terms E_{pw} , E_{www} and E_{NU} are energy redistribution terms due to pressure, convective motions and viscous stresses, respectively, producing no net integrated change over the entire layer. Note that the dissipation term may be decomposed as

$$\nu \langle (\partial_i u'_j + \partial_j u'_i) \partial_i u'_j \rangle = \nu \langle (\partial_i u'_j) (\partial_i u'_j) \rangle + \nu \langle (\partial_j u'_i) (\partial_i u'_j) \rangle.$$

Often in the literature the first term in this decomposition is termed dissipation, and the remaining term is added to the viscous diffusion term E_{NU} . This procedure is not generally correct since it is easily shown that $\langle (\partial_i u'_j) (\partial_i u'_j) \rangle$ is non-zero, for example for rigid-body rotation when the viscous dissipation is zero. For this reason we use the definition of dissipation in (8), which does not lead to such inconsistencies.

The thermal variance equation is

$$\begin{aligned}
 \partial_t \langle T'^2 \rangle &= -2 \langle w' T' \rangle \partial_z \langle T \rangle & T_{PRD} & \text{Production} \\
 &- 2\kappa \langle \partial_i T' \rangle (\partial_i T') & T_{DISS} & \text{Dissipation} \\
 &-\partial_z \langle w' T'^2 \rangle & T_{Tw} \\
 &+ \kappa \partial_z^2 \langle T'^2 \rangle & T_{DIFF} & \text{Diffusion.}
 \end{aligned} \tag{9}$$

The term T_{PRD} describes production of the temperature variance by the buoyancy forces, T_{DISS} is its dissipation and the terms T_{Tw} and T_{DIFF} are the redistribution terms that, integrated over the entire layer of fluid, are zero. All terms in (9) are non-dimensionalized by $\Delta T^2 \kappa / d^2$.

We have also computed spatial energy and temperature spectra, dominant frequencies of the velocity and temperature field oscillations, time dependence of the Nusselt number, and the vertical structure of velocity and temperature variances.

3. Numerical methods and code validation

The numerical code used in this investigation was developed in collaboration with Professor Steven A. Orszag. It is a modification of the FLOGUN code developed originally by Orszag & Kells (1980) to study channel flows. Equations (5) with the boundary conditions (6) were solved using pseudospectral methods as described by Gottlieb, Hussaini & Orszag (1984). In the horizontal direction, the dependent variables are expanded in Fourier series, whereas in the vertical direction, a Chebyshev expansion is employed. Thus, velocity components are represented as follows:

$$\mathbf{u}(x, y, z, t) = \sum_{|k| < K} \sum_{|m| < M} \sum_{n=0}^N \hat{\mathbf{u}}(k, m, n, t) \exp\left(\frac{2\pi i k x}{L_x}\right) \exp\left(\frac{2\pi i m y}{L_y}\right) T_n(z), \quad (10)$$

with a similar representation for the temperature field. The original version of the FLOGUN code uses a full time-splitting scheme that is not divergence-free at the boundaries. This can create large errors in computed quantities near the boundaries (Gottlieb *et al.* 1984). For this reason we have employed the Green-function method on the pressure and viscous terms in (5a) as described by Marcus (1984). This method correctly imposes implicit boundary conditions for pressure and avoids the difficulties of the full time-splitting scheme. Two additional fractional steps involve the Adams–Bashforth method on the nonlinear terms in (5) and the Crank–Nicolson method on the convective terms resulting from the decomposition of u and T into linear profiles and perturbations (formulae before (6)). The third fractional step in the temperature equation (5b) does not require the Green-function method and consists of the solution of the conduction equation. We have established that this method is second-order accurate in time. It requires about 1 s of CPU time on a Cray X-MP per time step for 32^2 (horizontal) \times 17 (vertical) modes and 7.5 s for $64^2 \times 33$ modes.

The code was tested by comparing the results it produced with results previously published in the literature. It was also tested for self-consistency by comparing steady-state solutions obtained from it for different initial conditions at the same Rayleigh number. The results for Nusselt numbers obtained in two- and three-dimensional runs without shear compared very well with the results given by Clever & Busse (1974). The two-dimensional simulations of convection with shear agreed qualitatively and quantitatively with the results of Lipps (1971).

We also ran simulations at the same Rayleigh numbers with different initial conditions: the velocity and temperature field initialized from the most unstable mode of the linear theory (Chandrasekhar 1961, p. 36) with the amplitude derived from Landau theory (Chandrasekhar 1961, p. 609) or a random temperature field with a white-noise spectrum and quiescent velocity field. Both initial conditions lead to the same final steady state, which is a good check of the self-consistency of our code.

4. Spatial and temporal resolution requirements

Before attempting direct numerical simulations of turbulent convection with shear, it is important to establish criteria for determining the spatial and temporal resolution necessary for accurate results. In the range of Rayleigh numbers amenable to direct numerical simulations ($Ra < 10^6$), the convection occurs in the form of dominant large-scale structures superimposed on small-scale turbulence. The

wavelength of the large-scale structures in free convection has been measured experimentally by Willis, Deardorff & Somerville (1972), Willis & Deardorff (1965) and Deardorff & Willis (1967), and their data are collected in a paper by Daly (1974). The requirement to accommodate in the computational domain at least one full large-scale structure imposes a lower limit on the periodicity lengths L_x and L_y . At the critical Rayleigh number $Ra_c = 1707.8$, the periodicity length should be $L \approx 2d$, growing to $L \approx 6d$ at $Ra = 6 \times 10^5$, according to figure 1 in Daly (1974). In numerical simulations, this condition is not always met (for instance, Eidson (1985) uses $L = 4d$ even for $Ra > 10^6$), leading to an increase in the computed heat flux over that measured experimentally. Also, according to Manley & Treve (1981) and Constantin *et al.* (1985), for qualitatively accurate numerical solutions of the hydrodynamic equations, the mesh should be fine enough to resolve dissipation eddies. A similar constraint on the average grid size was used by Grötzbach (1983):

$$h = (\Delta x \Delta y \Delta z)^{\frac{1}{3}} \lesssim \pi \eta_k \quad \text{for } Pr \leq 1, \quad (11)$$

where η_k is the Kolmogorov lengthscale. As will be discussed in §5.2, to get accurate results in our simulations it became necessary to use a stronger condition than (11), namely

$$\Delta x, \Delta y, \Delta z \lesssim \pi \eta_k \quad \text{for } Pr \leq 1. \quad (12)$$

Condition (12) should be applied away from the boundaries, where assumptions of homogeneous, isotropic turbulence are valid. In the vicinity of the boundaries, the resolution is determined by the necessity to resolve a thin conductive layer of depth $\delta_T \approx 1/(2Nu)$. Grötzbach (1983) suggests that at least three points are required in the conductive layer for turbulent convection, and Eidson *et al.* (1986) use a much higher resolution of eight points in the conductive layer.

The existence of the mean flow implies a viscous layer of depth $\delta_v \approx 1/(2Mo)$. Since, for Prandtl numbers around unity, the Nusselt number and the momentum number are of the same order of magnitude (Lipps 1971; Hathaway & Somerville 1986), $\delta_v \approx \delta_T$; therefore, resolution adequate for the conductive layer is also adequate for the viscous layer.

In this work we are interested in the interaction of shear with convection when both effects are comparable. Therefore, it is important to estimate the range of Richardson numbers for which energy production due to shear effects is comparable with the energy production due to buoyancy. The energy production by buoyancy forces takes place in a relatively uniform convective core and may be approximated as

$$E_c \approx \alpha g \langle T'w' \rangle d, \quad (13)$$

where $\langle T'w' \rangle$ is a value characteristic of the convective core (cf. equation (8)). The energy production due to shear is

$$E_s \approx -\langle u'w' \rangle \int_0^d \partial_z \bar{U} dz = u_*^2 \Delta \bar{U}, \quad (14)$$

where $-\langle u'w' \rangle = u_*^2$ is the approximately constant value of the momentum flux outside the viscous sublayer and $\bar{U}(z)$ is the mean velocity profile. From (13) and (14) and the requirement $E_s \approx E_c$, and assuming again that $Mo \approx Nu$, we get

$$|Ri| \approx Pr \quad (15)$$

as a condition for the global effects of shear and convection to be comparable.

To estimate time-step size, we found that it was convenient to use as a velocity

scale of convective motions an amplitude derived from Landau’s equation (Chandrasekhar 1961, p. 615),

$$A^2 = 160.46 \frac{\kappa^2}{d^2} \left(\frac{Ra}{Ra_c} - 1 \right), \quad (16)$$

even though Landau’s theory is formally valid only for $(Ra/Ra_c - 1) \ll 1$. The amplitude A scales in the same way as the characteristic velocity used by Deardorff (1970):

$$W_c^2 = g\alpha \Delta T d = \frac{\kappa\nu}{d^2} Ra. \quad (17)$$

Formula (16) was found to correspond more closely to the actual peak values of the convective velocity than (17) and, therefore, it was used for estimating time stepping. Based on (16), the large-eddy turnover time is

$$\tau \approx \pi d/A, \quad (18)$$

and for accurate results it was necessary to use between 200 and 500 time steps (depending on the Rayleigh number) for one large-eddy turnover time. In cases with large shear, the number of time steps must be increased owing to stability restrictions on advective terms in (5).

When simulations are initialized with a random temperature perturbation and a quiescent velocity field, convection develops in about two large-eddy turnover times. Usually one or two additional large-eddy turnover times are sufficient to achieve quasi-steady state, in which the flow evolution is much slower than in the transition period from the quiescent state to the convective state. For instance, Richter & Parsons (1975) measured the time t_s required for developed convection in high-Prandtl-number fluid to reach steady state after impulsively switching on mean shear. When their results are expressed in terms of the large-eddy turnover times τ , for moderate shear, $t_s \lesssim \tau$. Therefore, simulations should be run for about three to four large-eddy turnover times, corresponding to about 2000 time steps to reach quasi-steady flow. Nevertheless, it is not practical at present to perform numerical simulations of turbulent convection for more than a few thousand time steps.

5. Results of numerical simulations

5.1. Case specifications

It has been determined in the numerical simulations by Lipps & Somerville (1971) that transition from a quiescent state to fully developed convection is intrinsically a three-dimensional process. Even if the final state is purely two-dimensional, its characteristic wavelength is determined by the three-dimensional transient regime. For this reason, realistic numerical simulations of convection should be three-dimensional. Results reported later in this paper have been obtained from three-dimensional simulations.

It is known that in the case of convection without mean shear, transition to temporally aperiodic convection occurs at $Ra \approx 12000$ (Willis & Deardorff 1970), and convection becomes progressively more complex in space as well as time for larger Rayleigh numbers. However, Willis & Deardorff (1965) infer from their experiments that ‘the dominant organized motions retain their identity even for $Ra = 1.5 \times 10^6$ ’. Therefore, increased complexity of convection for increasing Rayleigh numbers is reflected mainly in the time dependence of convection rather

Run	IC	Ra	Ri	L_x	L_y	N	τ	t	Δt	N_t
1	0	35840	$-\infty$	8	8	$32^2 \times 17$	0.22	1.66	0.0014	1000
2	1	35840	$-\infty$	2.67	2.67	$32^2 \times 17$	0.22	1.12	0.0007	1600
3	0	35840	-2.0	8	8	$32^2 \times 17$	0.22	1.67	0.0014	2100
4	3	35840	-2.0	2.67	2.67	$32^2 \times 17$	0.22	0.56	0.0007	800
5	0	35840	-0.2	8	8	$32^2 \times 17$	0.22	1.12	0.0014	800
6	5	35840	-0.2	2.67	2.67	$32^2 \times 17$	0.22	0.75	$\left. \begin{array}{l} 0.0005 \\ 0.0003 \\ 0.0001 \end{array} \right\}$	2600
7	0	150000	$-\infty$	5	5	$64^2 \times 33$	0.10	0.4	0.0002	2000
8	7	150000	-0.2	5	5	$64^2 \times 33$	0.10	0.18	0.00006	3000
9	0	630000	$-\infty$	5	5	$64^2 \times 33$	0.051	0.20	0.0001	2000
10	9	630000	-0.3	5	5	$64^2 \times 33$	0.051	0.05	$\left. \begin{array}{l} 0.0001 \\ 0.00005 \\ 0.00003 \end{array} \right\}$	1000

TABLE 1. Simulation parameters. IC, Initial condition: 0, random initial condition; n , initial velocity and temperature field from the last time step of run n . Ra is the Rayleigh number, Ri the Richardson number, L_x and L_y the horizontal periodicity lengths in terms of the channel width a ($= 1$), N the number of horizontal and vertical Fourier modes in the simulation, τ the large-eddy turnover time, t the total time for the simulation, Δt the time step, and N_t the total number of time steps.

than in its spatial structure. The term ‘turbulent convection’ as used in this paper refers to the occurrence of significant aperiodicity in the time domain with the understanding that the flow may still appear to be quite organized in the spatial domain. In this sense, convection is turbulent for Rayleigh numbers above 12000.

Table 1 gives specifications for the cases that were run. All cases in table 1 have Rayleigh numbers in the turbulence range above 12000. Runs 1–6 are for $Ra = 35840$, which is the same as in the two-dimensional simulations of convection with shear performed by Lipps (1971). Runs 7 and 8 are for $Ra = 150000$, which was the highest Rayleigh number that could be simulated accurately. Runs 9 and 10 are for $Ra = 630000$, which corresponds to experimental results of Deardorff & Willis (1967). The resolution used in runs 9 and 10 was inadequate for highly accurate results. However, we found that computed physical quantities outside boundary layers were in fair agreement with experiments, and we felt it was worthwhile to report this finding. In most cases, absolute values of Richardson numbers were slightly lower than the estimate (15).

The choice of the aspect ratio of the computational domain represented a compromise between making the domain large enough to contain the largest eddies that drive the flow and maintaining sufficient spatial resolution to simulate accurately a range of the smaller eddies generated by these large eddies. In all runs, the distance between plates was set to $d = 1$. In runs 1, 3 and 5 the horizontal dimensions of the convective layer were chosen to accommodate two large-scale structures observed by Lipps (1971) in his two-dimensional simulations with shear at the same Rayleigh number. These dimensions are also equal to approximately twice the natural wavelength of convection without shear at this Rayleigh number (Daly 1974, figure 1). The size of the computational domain for $Ra = 150000$ is equal to approximately one natural wavelength of convection, and for $Ra = 630000$ it is about 20% less than the natural wavelength observed experimentally (Daly 1974,

figure 1). The large-eddy turnover times decrease by about a factor of 2 as the Rayleigh number is increased by factors of 4 from $Ra = 35840$ to $Ra = 150000$ and $Ra = 630000$. The integration time of the simulations extends for at least four large-eddy turnover times for runs 1, 7 and 9 without shear. For large Rayleigh numbers (runs 8 and 10), simulations with shear were restarted from the final fields obtained in runs 7 and 9 without shear. For that reason, the time of simulation in these cases is less than four large-eddy turnover times. Note that the time step in the shear cases is lower than in corresponding cases without shear, which is related to the numerical stability conditions on the advective terms in (5). The total number of time steps to complete these runs varies between 1000 and 3000.

5.2. Simulations for $Ra = 35840$

Runs 1, 3 and 5 were initialized assuming random temperature perturbations with a white-noise spectrum and either a quiescent velocity field or a linear mean velocity profile:

$$U(z) = z\Delta U, \quad -\frac{1}{2} \leq z \leq \frac{1}{2}$$

for the shear runs 3 and 5. When condition (11) is used in the middle of the channel in a form given by Grötzbach (1983, p. 251), one obtains for $Ra = 35840$

$$h \lesssim 0.2. \quad (19)$$

The maximum value of our average grid size for runs 1, 3 and 5 was $h = 0.185$ satisfying condition (19). The thickness of the thermal boundary layer was

$$\delta_T = \frac{1}{2} \frac{1}{Nu} \approx 0.14,$$

assuming $Nu \approx 3.5$. With the Chebyshev spacing in the vertical direction, we have three mesh points in the thermal boundary layers, excluding points at the boundaries $z = -\frac{1}{2}$ and $z = +\frac{1}{2}$. Therefore, the spatial resolution requirements discussed in §4 are apparently satisfied. Surprisingly, convection was dominated by three rather than two large-scale structures in the computational domain. Detailed analysis of runs 1, 3 and 5 revealed that the smallest scales were not accurately simulated, and the reason was traced back to an inadequate spatial resolution. Velocity and temperature spectra of the calculated flows decayed only by about one order of magnitude, and it became necessary to use a stronger condition than (11), namely condition (12). This was done by restarting low-resolution runs 1, 3 and 5 with the same number of modes ($32^2 \times 17$) and decreasing lengths L_x and L_y by a factor of 3 to preserve only one of the three large-scale structures that developed in these runs (denoted in table 1 as 2, 4 and 6). The contour plots of the velocity fields that developed at the ends of runs 2, 4 and 6 are shown in figures 2(a), 2(b) and 2(c), respectively.

In run 2, large-scale structures are organized in the y -direction. They have an appearance of rolls deformed in a wave-like pattern. In run 4, the rolls are organized in the x -direction, which is also the direction of the mean velocity. The deformation of the rolls is less in this case than in the previous one. Finally, in run 6, the large-scale convective structures have the appearance of almost perfect rolls aligned in the direction of the mean velocity. The level of organization of the convective cells is best

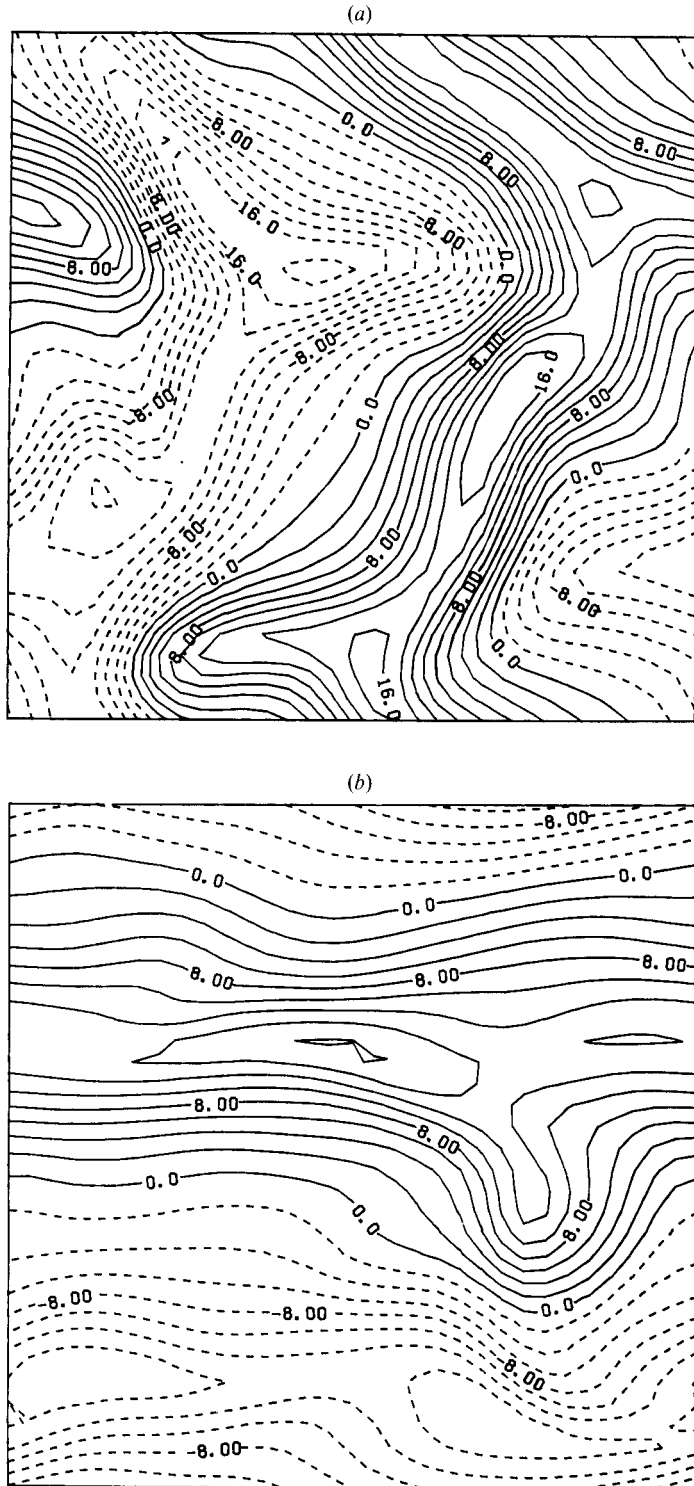


FIGURE 2(a,b). For caption see facing page.

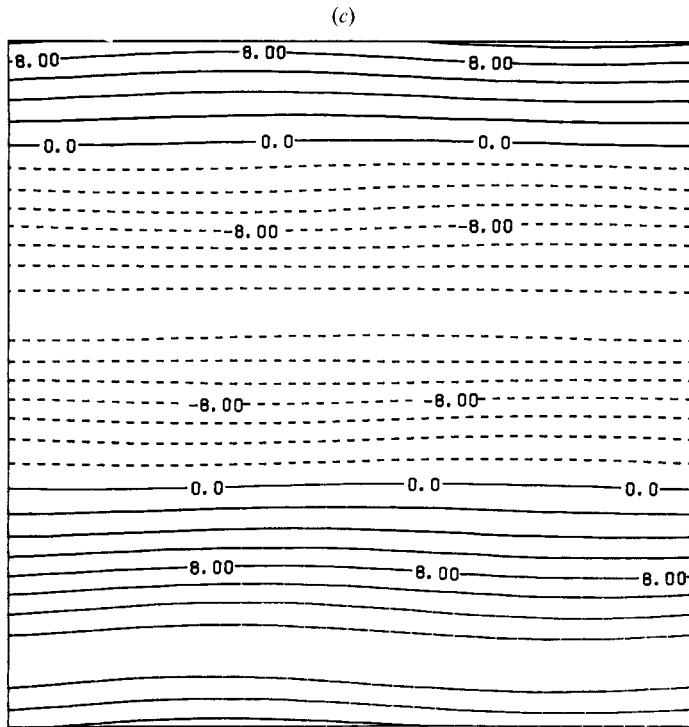


FIGURE 2. Contour plot of the vertical velocity w' in the plane $z = 0$. (a) Run 2: $Ra = 35\,840$, $Ri = -\infty$, $t = 2.5$. (b) Run 4: $Ra = 35\,840$, $Ri = -2.0$, $t = 2.0$. (c) Run 6: $Ra = 35\,840$, $Ri = -0.2$, $t = 1.8$. Here and in the subsequent figures the solid lines correspond to positive values and dotted lines to negative values.

described in terms of the longitudinal spectra of the velocity and temperature fields:

$$S_w(k, y, z) = \left| \frac{1}{2\pi} \int e^{-ikx} w'(x, y, z) dx \right|^2, \quad (20a)$$

$$S_T(k, y, z) = \left| \frac{1}{2\pi} \int e^{-ikx} T'(x, y, z) dx \right|^2, \quad (20b)$$

assuming rolls aligned in the x -direction. The spectra plotted in figures 3(a) and 3(b) for runs 2 and 6 are averaged over either the y - or x -direction and over several z -planes in the middle of the computational box. In run 2, the spectra in the x - and y -directions (figure 3a) are quite similar, indicating that there is a large degree of isotropy, especially for small scales (large k) in this run. In run 6, the spectrum averaged over the x -direction contains much less energy than the spectrum averaged over the y -direction (figure 3b). This is a reflection of the high level of organization of the convective rolls in this run. We may conclude from these figures that the main qualitative effect of shear is to organize rolls in the direction of the mean velocity with the level of organization increasing for increased shear. This behaviour is in agreement with the results of experiments by Hart (1971) and Sparrow & Husar (1969) performed on an inclined heated plate, by Ingersoll (1966) performed in a cylindrical container with a rotating lid and by Richter & Parsons (1975) performed in a recirculating plane Couette flow. Numerically similar results were obtained by Hathaway & Somerville (1986).

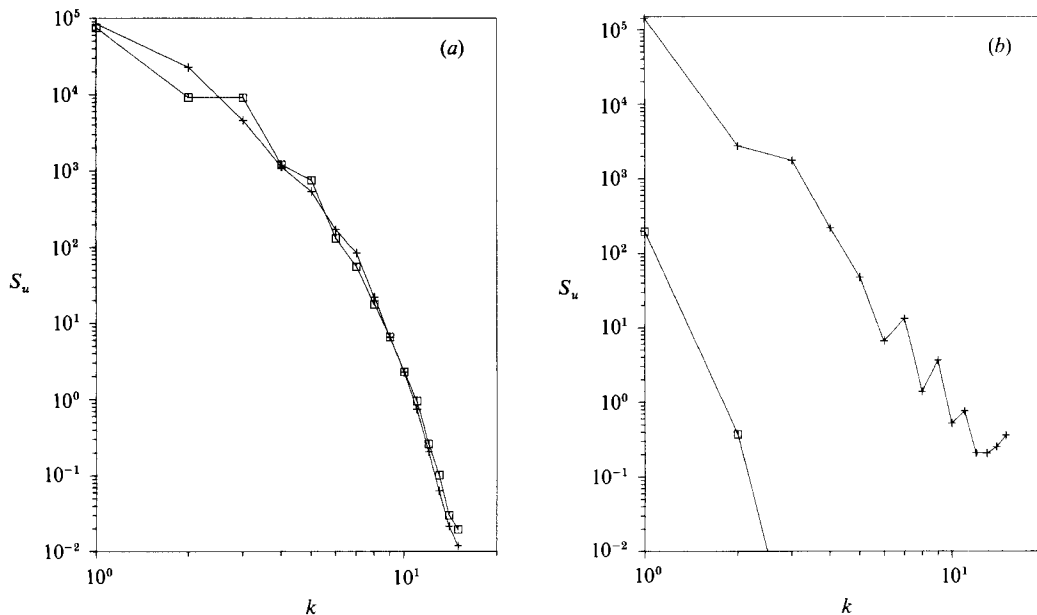


FIGURE 3. Velocity spectra in the horizontal directions as a function of wavenumber k : \square , x -direction; $+$, y -direction. (a) Run 2: $Ra = 35840$, $Ri = -\infty$. (b) Run 6: $Ra = 35840$, $Ri = -0.2$.

The complex time dependence of the flow is reflected in the behaviour of the time series of vertical velocity and temperature measured at specific points within the convective layer. Typical time series for run 2 are shown in figure 4. It is seen that the flow is aperiodic, as expected. Note the correlation between the temperature and vertical velocity, reflecting the downflow of the cold plumes† and the upflow of the hot ones. Since the time series are relatively short, no spectral analysis was attempted. The behaviour of the time series for the shear runs 4 and 6 was quite similar, indicating that the time dependence of the flow is caused primarily by the convective processes and is only marginally affected by the presence of the shear. This time dependence of the velocity and temperature fields results in the time dependence of spatially averaged quantities like the Nusselt number. The values of the Nusselt number (7a) computed in the middle of the layer ($z = 0$) and near the upper boundary ($z = 0.46$) for run 2 are shown in figure 5 as a function of time. In a perfectly steady state, the Nusselt numbers at both locations should be equal and independent of time. Instead, they oscillate, with the amplitude of oscillation at $z = 0$ about a factor of 3 larger than the amplitude at $z = 0.46$. The peak in the Nusselt number at $z = 0$ always precedes the peak in the Nusselt number at $z = 0.46$. This behaviour was found also for higher Rayleigh numbers and the shear cases.

Our simulation results are consistent with a model of the flow based on the dynamics of large-scale, quasi-two-dimensional, counter-rotating vortical cells. Similar models have been previously proposed in the literature (e.g. Veronis 1966). There appears to be an inherent dynamical instability in this cellular motion, as evidenced by the temporal oscillations in the Nusselt number (figure 5) and in a similar behaviour of other terms in the energy-balance and temperature-variance

† In this paper we use the terms ‘plume’ and ‘thermal’ in the sense defined by Turner (1973). A ‘plume’, or buoyant jet, is a continuous buoyant region between the two plates, while ‘thermal’ refers to an isolated volume of buoyant fluid detached from its source.

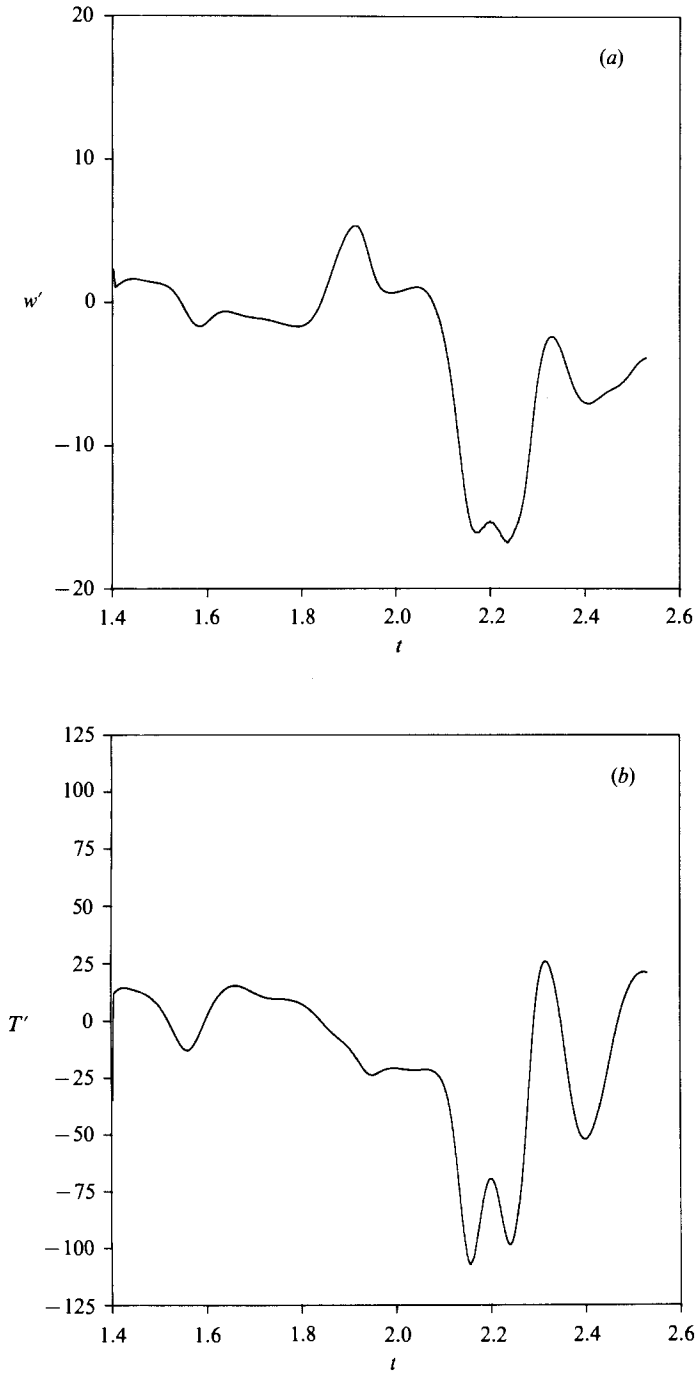


FIGURE 4. Time series of vertical velocity and temperature at two points inside the convective layer for run 2. (a) Vertical velocity w' at $x = 0.5L_x$, $y = 0.5L_y$, $z = 0$. (b) Temperature T' at $x = 0.5L_x$, $y = 0.5L_y$, $z = 0$.

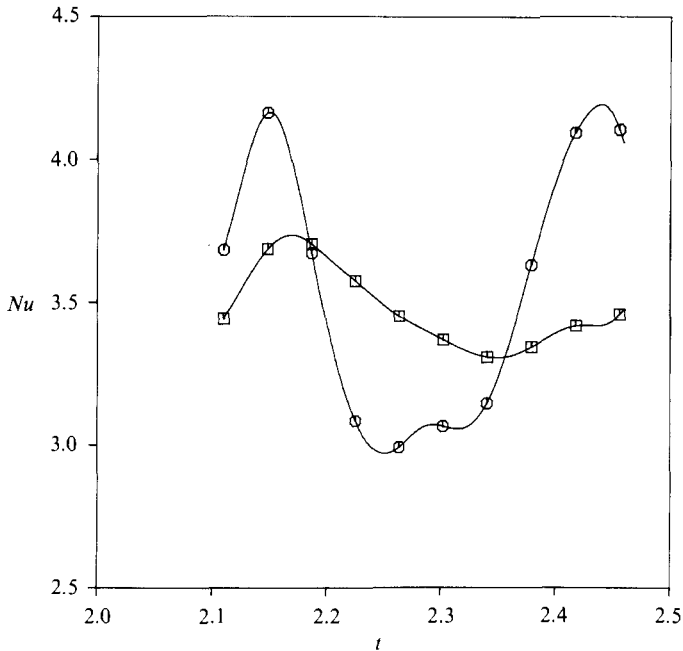


FIGURE 5. Nusselt number as a function of time at two different z -levels: \square , $z = 0.46$; \circ , $z = 0$; for Run 2, $Ra = 35840$, $Ri = -\infty$.

equations (8) and (9). If an excess of heat develops at the lower boundary, it is drawn into the rising plume between the two cells and tends to enhance the vortical motion while increasing the Nusselt number in the middle of the channel. When the temperature anomaly reaches the top boundary, the Nusselt number will then attain a peak value there, after the peak at the middle of the channel (cf. figure 5). If, as the cellular motion spreads the excess hot fluid along the top boundary, the heat flux through the boundary is insufficient to return this fluid to the wall temperature, the inertial motion of the vortex cells will then begin pumping relatively hot fluid back down toward the bottom. If this effect is strong enough, it can create a reversal in the mean temperature gradient and a reduction of the Nusselt number in the middle of the channel and reduce the rotation rate of the large eddies. This, in turn, will foster the development of another temperature anomaly at the bottom boundary, and the cycle will repeat, with the cells being alternately driven by buoyancy and inertial effects.

Our simulations exhibit just such a time-varying reversal of the mean temperature gradient in the middle of the channel. Such effects have also been seen experimentally (e.g. Chu & Goldstein 1973) at Rayleigh numbers $Ra \lesssim 10^6$, although not at higher Rayleigh numbers. There is also a temporal variation in perturbation kinetic energy and heat flux, consistent with the above model.

In table 2, we have gathered time-averaged Nusselt numbers and apparent periods of oscillation for our runs. The periods are based on data extending for only about one full oscillation and must be interpreted with caution. However, it is clear that they are the same order of magnitude as the large-eddy turnover times. The oscillations of the Nusselt number in our simulations appear to be dynamically linked to the largest-scale structures in our computational domain. Statistical averages

Run	Ra	Ri	Nu	τ	T_p	Mo
2	35 840	$-\infty$	3.51	0.22	0.36	—
6	35 840	-0.2	3.54	0.22	0.20	4.02
7	150 000	$-\infty$	5.30	0.10	0.18	—
8	150 000	-0.2	4.38	0.10	0.15	5.64
9	630 000	$-\infty$	7.60	0.051	0.09	—
10	630 000	-0.3	5.80	—	—	—

TABLE 2. Heat and momentum fluxes. Nu and Mo are the normalized heat and momentum fluxes [equation (7)], and T_p is the apparent period of oscillation of these quantities.

computed over a large number of such convective cells that were not phase correlated would tend to be uniform in time.

This unsteady process of the heat transfer is somewhat similar to the heat transfer in high-Rayleigh-number flows, where heated fluid is first accumulated in the vicinity of the boundary and is later released rapidly in the form of a buoyant thermal (Townsend 1959). For high-Rayleigh-number flows, the unsteady character of the heat transfer is also expected from Howard's (1964) theory. The unsteadiness of the heat flux may contribute to the large scatter of experimentally measured instantaneous Nusselt numbers. In fact, Deardorff & Willis (1967) report that instantaneous Nusselt numbers may differ by as much as 50% from their time and vertically averaged values, though they attribute these differences to inequality between averages taken along horizontal lines and averages taken over entire horizontal planes.

Experimental results for $Ra = 35\,840$ give a Nusselt number lower than our run 2 ($Nu = 3.10$ for air (Brown 1973), $Nu = 3.20$ for helium (Threlfall 1975)). This can be explained by the fact that the size of the computational domain, $L = 2.67$, is less than the natural wavelength of the convection, $L \approx 4$ (Daly 1976) at this Rayleigh number. The use of inadequate horizontal dimensions led consistently to higher than experimental heat fluxes in the numerical simulations of Grötzbach (1982, 1983) and Eidson (1985).

When runs 2 and 6 are compared, we see a slight increase in the Nusselt number in the shear run 6. This increase of less than 1% is probably not significant, since differences in Nusselt numbers for different flow realizations and the same external conditions are usually larger than 1%. However, Hathaway & Somerville (1986) report a similar trend of a slight increase in the heat flux for increased shear in their simulations of convection at $Ra = 10\,000$. Convection without mean shear at both $Ra = 10\,000$ and $Ra = 35\,840$ has a spatial structure more complicated than the strictly two-dimensional roll pattern characteristic of steady convection just above the critical point (see figure 2*a*). Strong enough shear, however, increases the level of organization of the convective cells, as seen in figure 2(*c*), and this may explain the increased heat transfer with higher shear. This is consistent with results of Grötzbach (1982, runs 7–11) and Daly (1974, figure 2), who found that the Nusselt number for three-dimensional convection at a given Rayleigh number is lower than the Nusselt number for convection forced to be two-dimensional at the same Rayleigh number.

For the shear runs 6 and 8 we have also computed the non-dimensional momentum flux Mo . It was found that the momentum flux fluctuated in time in the same manner as the heat flux. Averaged values of Mo are greater than averaged values of Nu by

10–30% (table 2). For two-dimensional convective rolls parallel to the mean velocity, theory predicts that $Mo = Nu$ (Lipps 1971) when $Pr = 1$. Since we have $Pr = 0.71$, our results are only in approximate agreement with this prediction. It should also be noted that the two-dimensional simulations of Lipps (1971) indicate that $Mo \geq Nu$ for $Pr \leq 1$ and $Mo < Nu$ for $Pr > 1$. Our results indicate that for $Pr < 1$, $Mo > Nu$ holds for three-dimensional convection as well.

The individual terms in the kinetic-energy-balance equation are shown in figure 6(a–d). In run 2, without shear, the energy production takes place in the convective core and dissipation is large in the vicinity of the boundaries. In run 6, the energy production by buoyancy forces and the dissipation are controlled by the value of the Rayleigh number and are affected very little by the shear. The energy production by the shear is concentrated in the boundary layers where the effects of buoyancy are small. The total energy production by the shear in this run is about 1.5 times greater than the total energy production by the buoyancy. In both runs, a very important term in the energy-balance equation is the conservative pressure diffusion term E_{pw} . Its main role is to transfer energy produced by the buoyancy inside the convective layer towards the boundaries where it is dissipated by the dissipation term E_{DISS} . The pressure diffusion term E_{pw} is quite often neglected or lumped together with the convective diffusion term E_{www} in the turbulence models. Monin & Yaglom (1979, p. 401) state that the pressure diffusion terms are ‘more often than not ignored... because they are almost always unknown’. Mellor & Yamada (1982) set the pressure diffusion term to zero, though the term E_{www} is retained in their analysis. In the experimental results of Deardorff & Willis (1967), the term E_{pw} was not measured individually, but only the sum $E_{pw} + E_{www}$ was calculated as the residual of other terms in the kinetic-energy budget. Similarly, the sum $E_{pw} + E_{www}$ was calculated by Lipps (1976) in his numerical simulations. The results presented in figures 6(b) and 6(d) indicate that the pressure diffusion term is generally greater than the convective diffusion term E_{www} . This is especially true in the case of run 2 without mean shear, where the convective diffusion is negligible in comparison with the pressure diffusion. These results suggest that the pressure diffusion should be modelled more carefully than is generally the practice in existing turbulence models. The importance of pressure diffusion in modelling the turbulent boundary layer was also recognized recently in the experimental work of Deardorff & Willis (1985). The effects of shear are most pronounced in the viscous diffusion term E_{NU} in the boundary layers where viscous diffusion is the basic physical mechanism for transferring the energy produced by the shear towards rigid boundaries where it is dissipated. The large values of viscous diffusion and viscous dissipation in the boundary layers are related to the large velocity gradients at the boundaries.

5.3. $Ra = 150000$

With a resolution of $64^2 \times 33$ modes, we could accurately simulate flows with a maximum Rayleigh number around 150000. Run 7 was initialized with a random temperature perturbation and was run for 2000 time steps. Run 8 was restarted from the results of run 7 at the last time step, switching on shear adiabatically until the Richardson number reached the value $Ri = -0.2$. Contour plots of the velocity fields for both runs at $z = 0$ are shown in figures 7(a) and 7(b). In run 8, with non-vanishing mean velocity, the large-scale structures are organized in the direction of the velocity. This time, however, the level of organization is lower than in run 6, which had the same Richardson number, $Ri = -0.2$, but a lower Rayleigh number, $Ra = 35840$. This increased randomness may be partially explained by the fact that

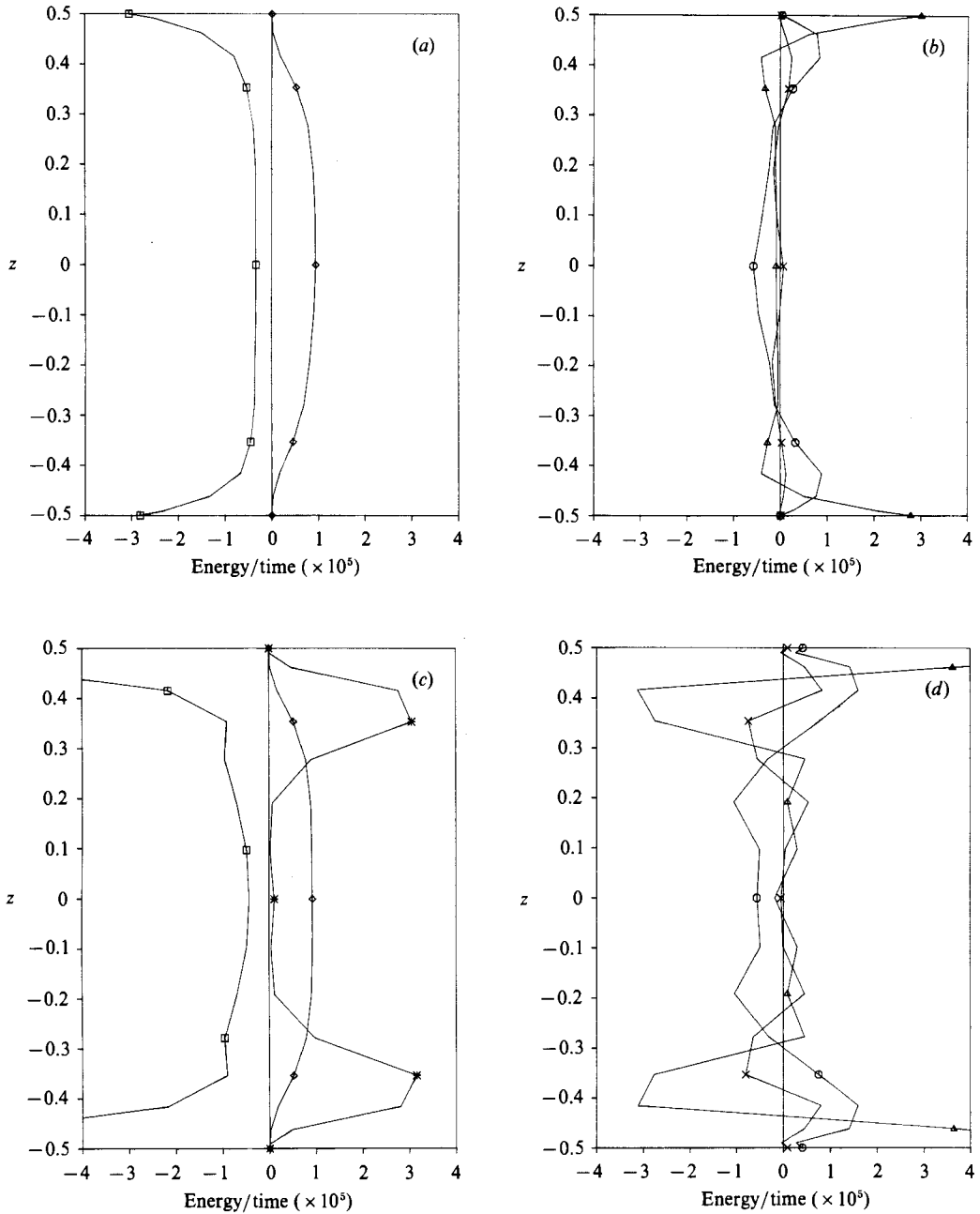


FIGURE 6. The vertical structure of the terms in the kinetic-energy-balance equation: \square , dissipation, $\nu\langle(\partial_i u'_j + \partial_j u'_i)\partial_i u'_j\rangle$; \diamond , production due to buoyancy, $\alpha g\langle T'w'\rangle$; $*$, production due to shear, $-\langle u'_i u'_k\rangle\partial_k\langle u'_i\rangle$; \circ , pressure diffusion, $-\partial_k\langle pu'_k\rangle$; \triangle , viscous diffusion, $\nu\partial_i\langle u'_j(\partial_j u'_i + \partial_i u'_j)\rangle$; \times , convective diffusion, $-\frac{1}{2}\partial_k\langle q^2 u'_k\rangle$. (a) Production and dissipation terms for run 2: $Ra = 35840$, $Ri = -\infty$, $t = 2.4$. (b) Redistribution terms for run 2. (c) Production and dissipation terms for run 6: $Ra = 35840$, $Ri = -0.2$, $t = 1.8$. (d) Redistribution terms for run 6.

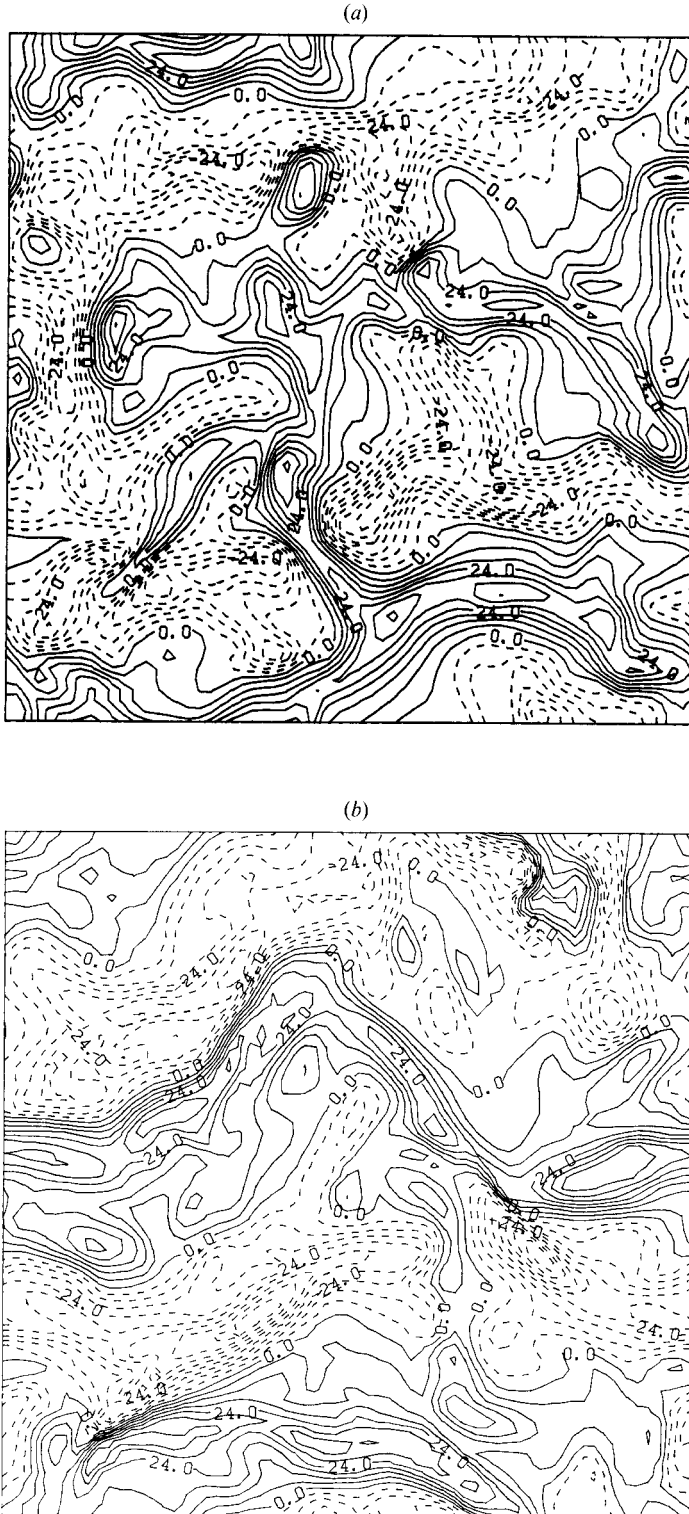


FIGURE 7. Contour plot of vertical velocity w' in the plane $z = 0$. (a) Run 7: $Ra = 150000$, $Ri = -\infty$, $t = 0.4$. (b) Run 8: $Ra = 150000$, $Ri = -0.2$, $t = 0.12$.

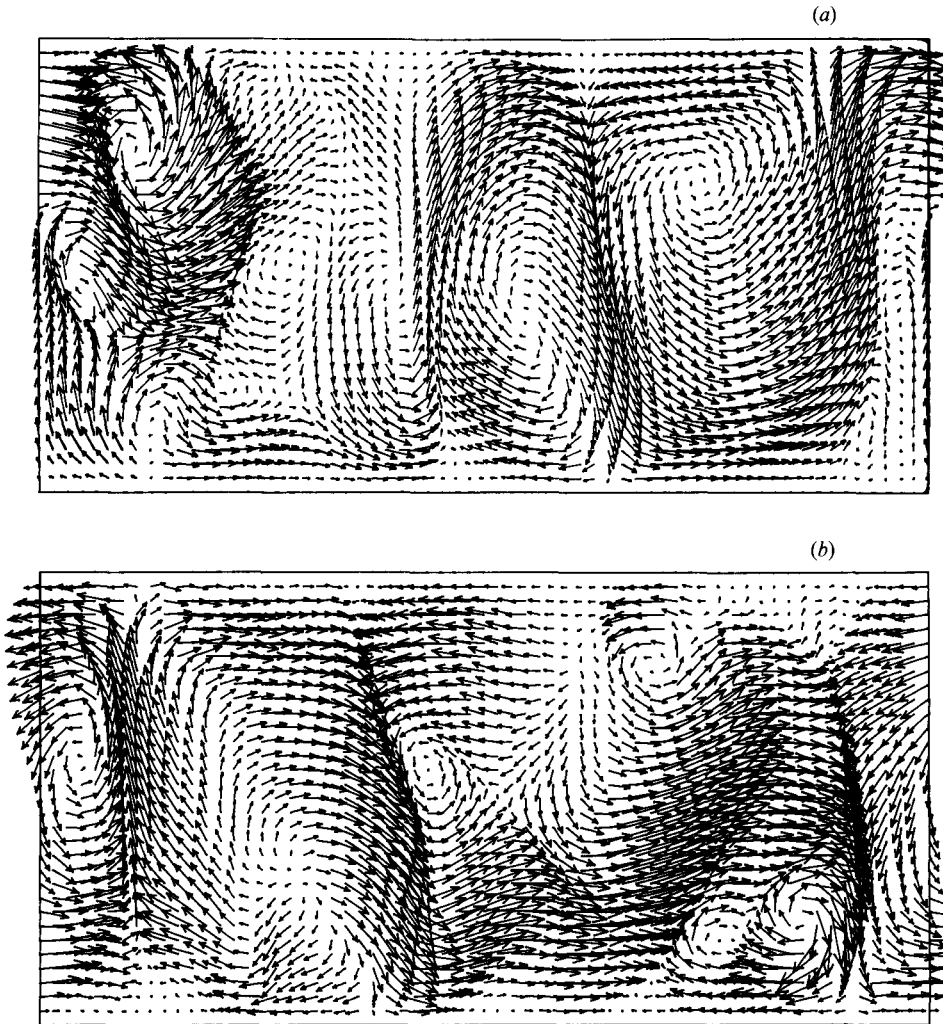


FIGURE 8. Vector plots of the perturbation velocity in the vertical planes. (a) Run 7: $Ra = 150000$, $Ri = -\infty$, $t = 0.4$. Vertical $(0xz)$ -plane at $y = 0.5L_y$. (b) Run 8: $Ra = 150000$, $Ri = -0.2$, $t = 0.12$. Vertical $(0yz)$ -plane at $x = 0.5L_x$. The ratio of the vertical to horizontal dimension is rescaled to the value 0.5.

in run 8 the ratio of the energy production due to shear to the energy production due to buoyancy forces is roughly 1 compared with 1.5 in run 6.

The structure of the velocity field is more complicated for $Ra = 150000$ than it was for $Ra = 35840$. Figures 8(a) and 8(b) show typical velocity fields for runs 7 and 8. These fields cannot be classified as simple deformed rolls, though remnants of the rolls may be seen in the right half of figure 8(a). The distinctive feature of these fields is the appearance of recirculating zones of fluid superimposed over each other vertically as in the left half of figure 8(a) and the right half of figure 8(b). When the vector plot of the velocity field in figure 8(a) is compared to the contour plot of the temperature field in figure 9(a), it is seen that these recirculating zones correspond to a cold plume descending from the upper plate and a cold thermal at the lower plate. The plume-like structure of the temperature field is apparent in figures 9(a) and 9(b), with most of the plumes extending throughout the entire depth of the

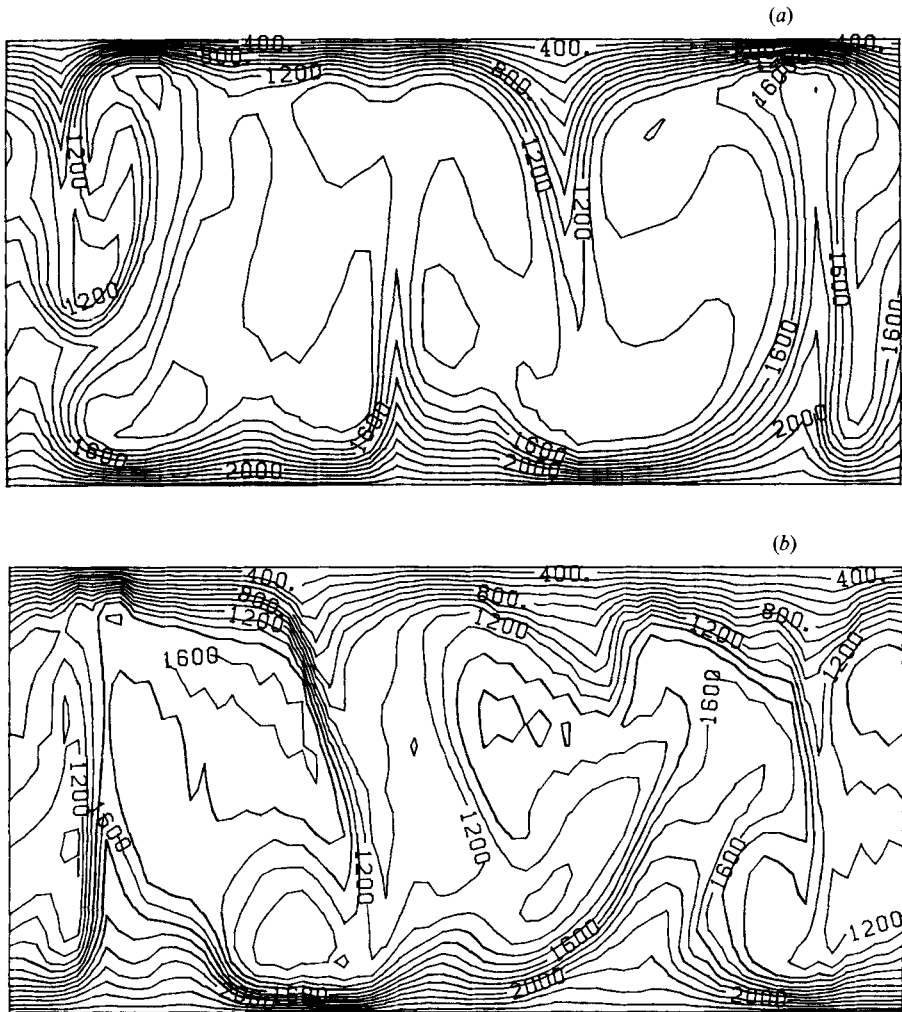


FIGURE 9. Contour plots of the temperature field T in the vertical planes. (a) See caption to figure 8(a). (b) See caption to figure 8(b). The ratio of the vertical to horizontal dimension is rescaled to the value 0.5.

convective layer. However, the plumes are less clearly defined in figure 9(b) than in figure 9(a), probably owing to the disruptive influence of shear.

The appearance of the recirculating zones of the fluid at this Rayleigh number helps to explain the fact that the Nusselt number is significantly greater in run 7 (without mean shear) than in run 8 (with mean shear). The contour plot of the temperature field for run 8 in the vertical plane along the direction of the mean velocity (figure 10) reveals the presence of closed contours tilted to the right. Such closed contours were also consistently observed at other planes oriented in this direction. There is evidence that some of those contours may be interpreted as thermals, i.e. regions of the colder (or hotter) fluid immersed almost entirely in a hotter (or colder) fluid and detached from the boundary. They originate from plumes in the convective layer that are torn off by the action of the shear. Since the thermals are immersed in the colder (hotter) fluid, they lose more heat to the surrounding fluid than does a continuous plume extending between the plates, which is more organized

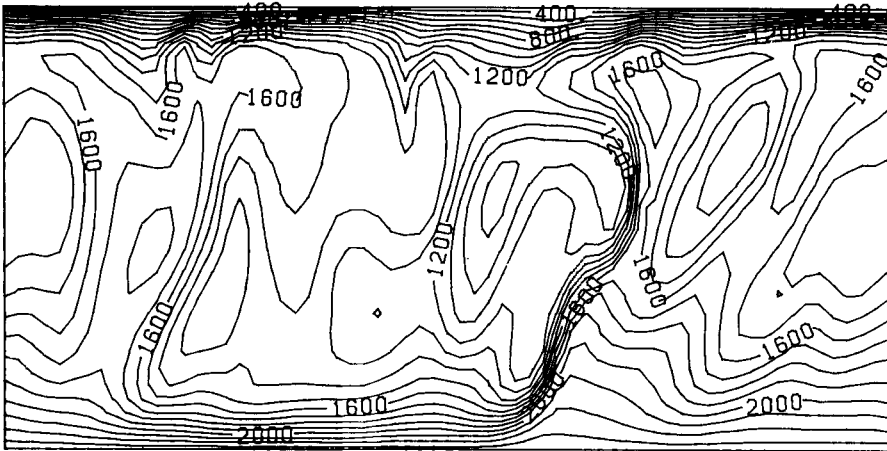


FIGURE 10. Contour plot of the temperature field T in the vertical (xz) -plane at $y = 0.5L_y$ for run 8: $Ra = 150000$, $Ri = -0.2$, $t = 0.12$. The ratio of the vertical to horizontal dimension is rescaled to the value 0.5.

in the vertical direction. Thus, it appears that the organized plume should be more effective in transferring heat from the lower to the upper plate than the plume distorted by the action of the shear. In fact, in our calculations we have seen that the normalized correlation $\overline{w'T'}/(\overline{w'^2T'^2})^{1/2}$ was always less for run 8 than for run 7, indicating that the flow is less organized in the presence of shear at this higher Rayleigh number. These processes lead on average to a decrease in the total heat transfer for convection with increasing shear. This reasoning is similar to the explanation given by Ingersoll (1966) to interpret results of his experiments that showed a decrease in the Nusselt number for increasing shear.

The difference in the efficiency of heat transfer between both cases is also reflected in the vertical profiles of the mean temperature shown in figure 11. The departures from the linear profile characteristic of the purely conductive states are smaller in shear run 8 than in run 7. In run 7, the convective core with an almost constant temperature consistently contained a small region in which a temperature-gradient reversal periodically occurred. This was not true for run 8. The behaviour of the mean velocity (figure 12) is quite similar to the behaviour of the mean temperature. It is almost constant in the convective core and changes rapidly in the boundary layers. The velocity-boundary-layer thickness is approximately the same as the temperature-boundary-layer thickness since $Pr = O(1)$.

The behaviour of the kinetic-energy-balance equation terms for $Ra = 150000$ (figure 13) is quite similar to the runs with $Ra = 35840$ (figure 6). The energy production is concentrated in the convective core (E_{Tw}) and in the velocity boundary layers (E_{uw}), and the dissipation is relatively uniform in the core and rapidly increasing close to the boundaries. Among the diffusive terms, the pressure diffusion E_{pw} is again quite important, reinforcing our conclusion from the previous section that there is little justification for neglecting this term in turbulence models.

The terms in the thermal-variance equation (9) are shown in figure 14. The temperature variance is produced mostly in the transition region between the thermal boundary layer and the convective core. The diffusive terms transfer it towards rigid boundaries and, to a lesser degree, to the core. The dissipation is almost

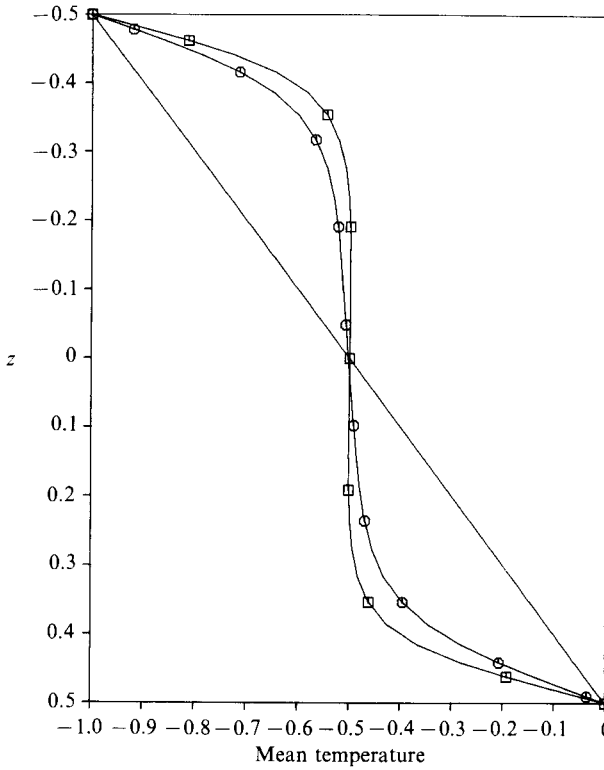


FIGURE 11. Vertical profiles of the mean temperature $(\langle T \rangle - (T_0 + \Delta T)) / \Delta T$: \square , run 7; \circ , run 8.

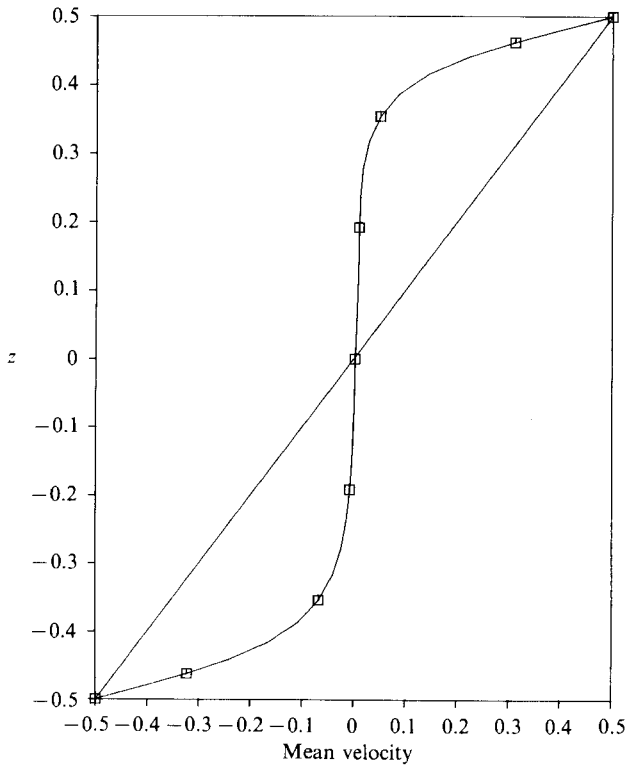


FIGURE 12. Vertical profile of the mean velocity $\langle u \rangle / \Delta U$ for run 8: $Ra = 150000$, $Ri = -0.2$.

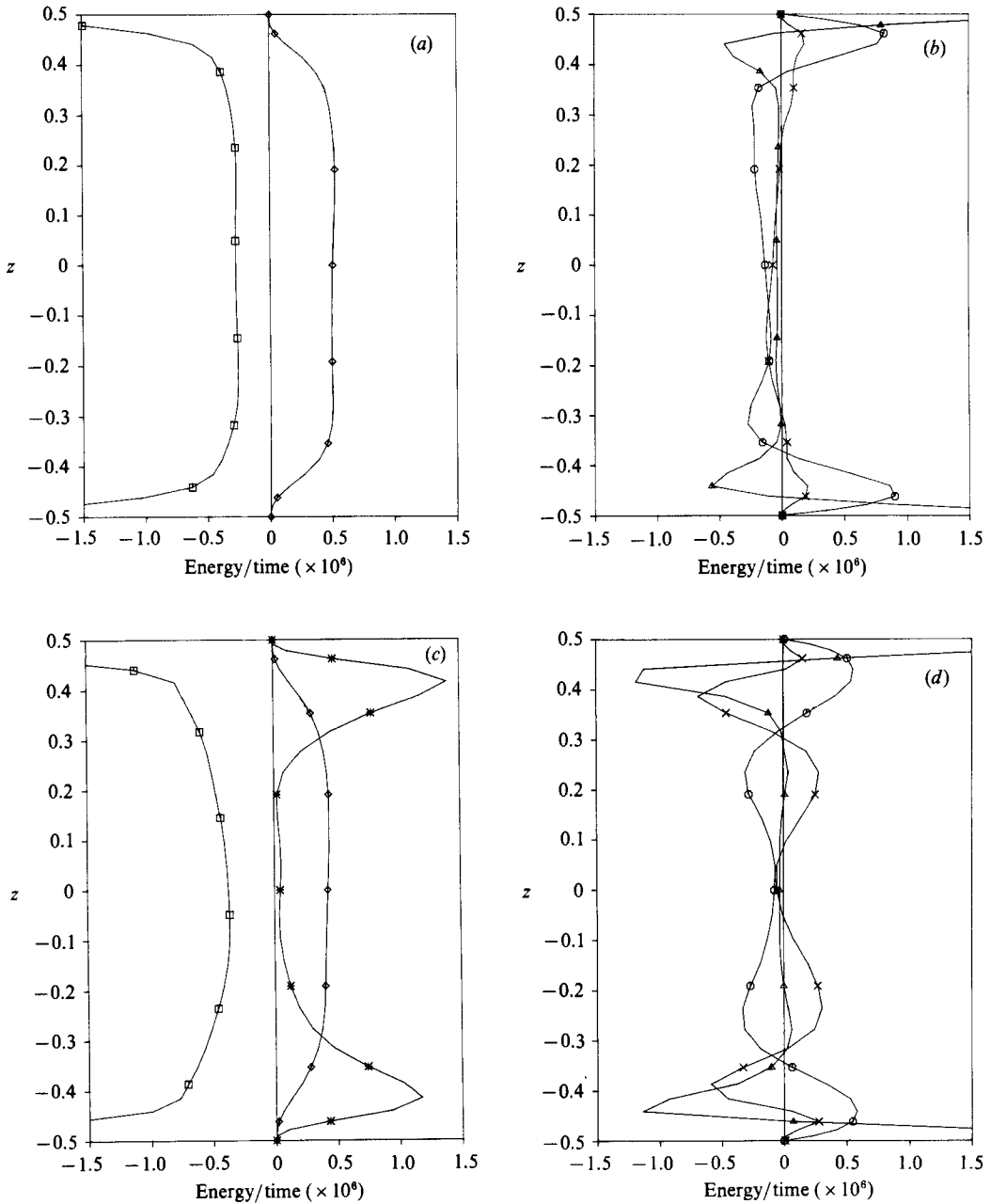


FIGURE 13. The vertical structure of the terms in the kinetic-energy-balance equation. For a description of the symbols, see caption to figure 6. (a) Production and dissipation terms for run 7: $Ra = 150000$, $Ri = -\infty$, $t = 0.4$. (b) Redistribution terms for run 7. (c) Production and dissipation terms for run 8: $Ra = 150000$, $Ri = -0.2$, $t = 0.18$. (d) Redistribution terms for run 8.

uniform in the core and increases by a factor of 3 throughout the thermal boundary layer. It is interesting to compare figure 14(a) with the corresponding figure 17 of Deardorff & Willis (1967) presenting the thermal-variance budget for $Ra = 630000$. The qualitative behaviour of the thermal variance budget is the same in both cases, including sign reversals in the diffusive terms in the boundary layer. However,

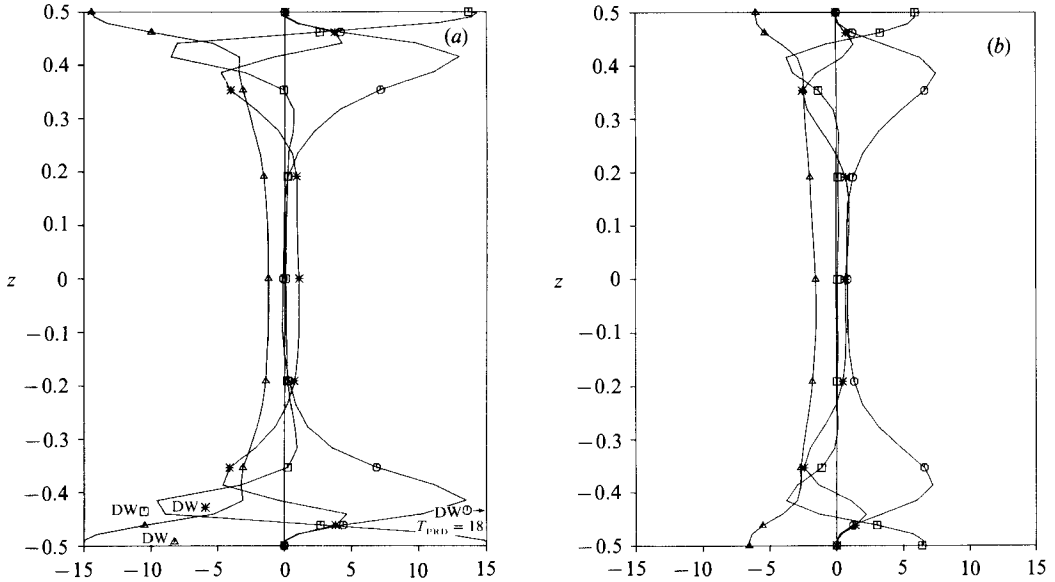


FIGURE 14. The vertical structure of the terms in the temperature-variance equation: \circ , production, $-2\langle w'T' \rangle \partial_z \langle T' \rangle$; \triangle , dissipation, $-2\kappa \langle (\partial_i T') (\partial_i T') \rangle$; \square , conductive diffusion, $\kappa \partial_z^2 \langle T'^2 \rangle$; $*$, convective diffusion, $-\partial_z \langle w'T'^2 \rangle$. (a) Run 7: $Ra = 150\,000$, $Ri = -\infty$, $t = 0.4$. Additional points (DW) on this plot represent peak values of those terms in experiments of Deardorff & Willis (1967) at $Ra = 630\,000$. (b) Run 8: $Ra = 150\,000$, $Ri = -0.2$, $t = 0.18$.

quantitative comparison is not as good. In figure 14(a), we marked positions of the peaks in T_{PRD} , T_{DISS} and T_{DIFF} taken from Deardorff & Willis (1967). It is seen that the absolute values of the production peak and the conductive diffusion peak are lower in our case than in their paper. This is due in part to the fact that they used a higher Rayleigh number than we did in our simulations. The absolute values of the conductive diffusion and the dissipation at the boundaries are substantially higher in the numerical simulations than in the experiments. Nevertheless, the numerical results for these quantities are self-consistent in the sense that the dissipation is exactly balanced by the molecular diffusion at the boundaries. A possible reason for this discrepancy between experimental and numerical results at the boundaries is inadequate spatial resolution in the boundary-layer region. It should also be noted that the experimental results may have errors on the order of $\pm 50\%$ in the boundary regions as reported by Deardorff & Willis (1967). Thus, the accuracy of the numerical simulations seems to be acceptable, though higher resolution in the boundary layers should be tried. The most striking difference between the thermal-variance budget for the runs with and without mean shear is a substantial decrease in the peak values of all terms for the shear case (figure 14b) without change in their qualitative behaviour as compared with the case without mean shear (figure 14a). This is explained by the previously discussed observation that one of the effects of the shear is to decrease the mean temperature gradients in the boundary regions (figure 11) and to broaden the thermal boundary layers. Since the same effect could be achieved without an application of the mean shear by reducing the Rayleigh number of the flow, we may view the action of the shear as effectively reducing the Rayleigh number. This should result in the lower Nusselt number and lower peak values of the terms in the temperature-variance equation.

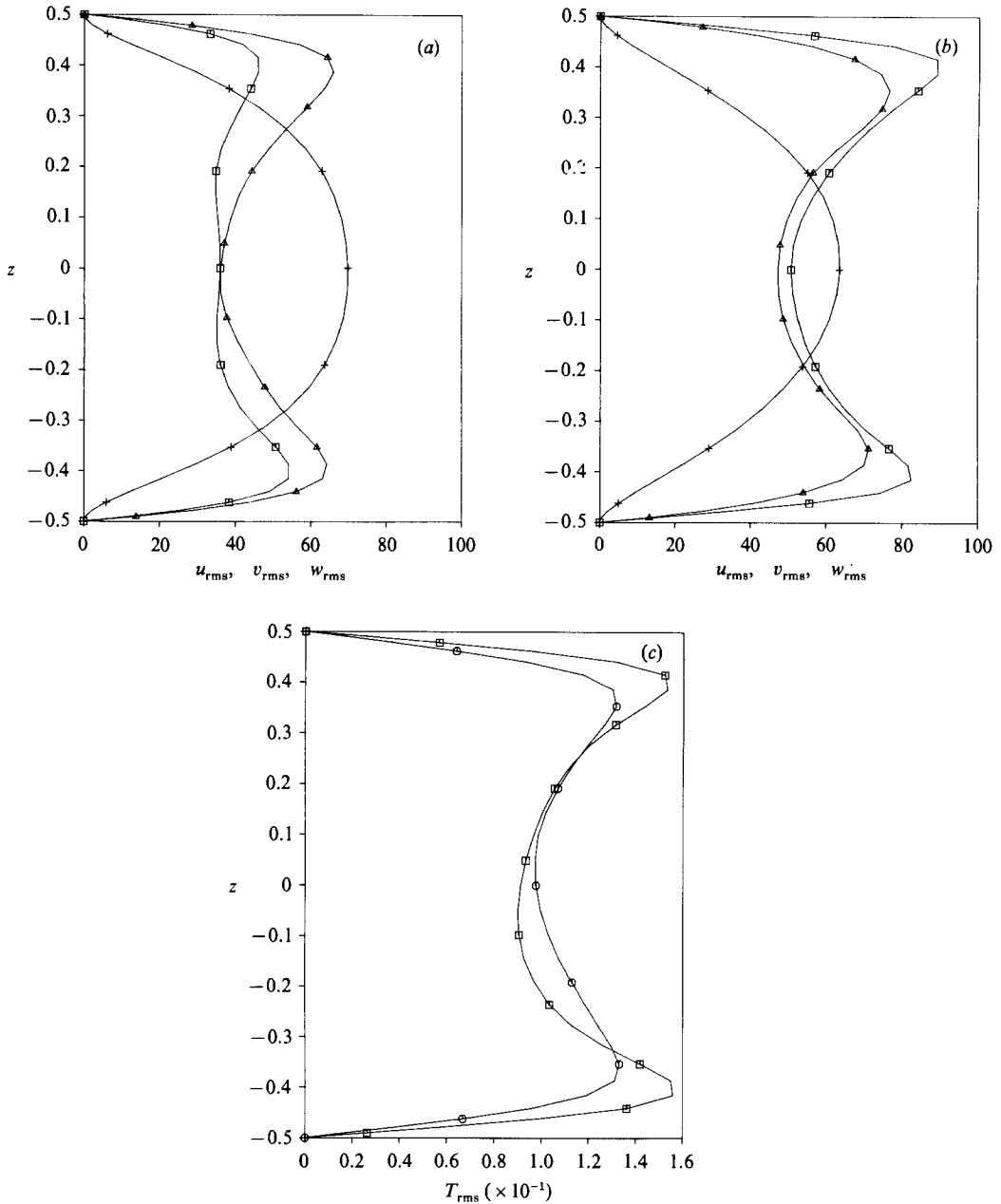


FIGURE 15. The vertical structure of the r.m.s. velocities and temperatures: \square , $u_{rms} = \langle u'^2 \rangle^{\frac{1}{2}}$; \triangle , $v_{rms} = \langle v'^2 \rangle^{\frac{1}{2}}$; $+$, $w_{rms} = \langle w'^2 \rangle^{\frac{1}{2}}$. (a) Run 7: $Ra = 150\,000$, $Ri = -\infty$, $t = 0.4$. (b) Run 8: $Ra = 150\,000$, $Ri = -0.2$, $t = 0.18$. (c) r.m.s. temperature $T_{rms} = \langle T'^2 \rangle^{\frac{1}{2}}$: \square , run 7; \circ , run 8.

Instantaneous vertical profiles of the r.m.s. velocities normalized by κ/d and temperature normalized by ΔT are plotted in figure 15. For the case with $Ri = -\infty$ the profiles have the same qualitative shape as obtained by Deardorff & Willis (1967). The vertical velocity reaches its peak in the middle of the convective layer, while the horizontal velocities and temperature have peaks in the boundary layers and decrease inside the convective core. Such behaviour is consistent with convection

Run	Ra	Ri	$w_{\text{rms}}/0.5(u_{\text{rms}} + v_{\text{rms}})$	References
2	35840	$-\infty$	1.01	—
7	150000	$-\infty$	1.17	—
8	150000	-0.2	0.67	—
—	630000	$-\infty$	1.14	(Deardorff & Willis 1967)
—	2500000	$-\infty$	1.07	(Deardorff & Willis 1967)

TABLE 3. Ratios of channel-averaged r.m.s. velocities

dominated by strong vertical plumes mushrooming in the boundary layers, as shown in contour plots of temperature (figures 10 and 11). The horizontal velocity field is not exactly isotropic, with the r.m.s. velocity in the y -direction generally greater than the r.m.s. velocity in the x -direction. The degree of anisotropy varies in time, and figure 15(a) depicts it close to a maximum level during our run. If profiles of the u_{rms} and v_{rms} were averaged over time, the degree of anisotropy would be lowered, though there always would be bias towards greater values of v_{rms} than u_{rms} . Some degree of anisotropy in our runs should be expected because our computational domain is too small to accommodate more than one large-scale structure, which generally will be anisotropic. The peak values of the r.m.s. velocities in figure 15(a) are about a factor of 2 less than corresponding values in figure 6 of Deardorff & Willis (1967). This ratio is consistent with the ratio of characteristic velocities estimated on the basis of the amplitude (16) for $Ra = 630000$ and $Ra = 150000$, respectively. The values of T_{rms} for the unsheared case in figure 15(c) are higher than in the experiments of Deardorff & Willis (1967) at $Ra = 630000$, but this is consistent with the trend towards higher T_{rms} with decreasing Rayleigh numbers seen in their experiments.

The qualitative shape of the curves for the shear case (figure 15b, c) is the same as in the case without shear. With shear, however, the values of the r.m.s. horizontal velocities are about 30% greater, so that the minimum of the r.m.s. horizontal velocities is approximately equal to the maximum of the r.m.s. vertical velocities. In general, the time-averaged r.m.s. horizontal velocities are quite isotropic. This is somewhat surprising since the anisotropy introduced by the mean velocity in the x -direction might lead one to expect that u_{rms} should be greater than v_{rms} . Apparently, the convective mixing must be very efficient in equalizing the horizontal components of the fluctuating velocity field. The ratios of the r.m.s. velocities averaged over the entire convective layer for runs 7 and 8 are compared in table 3 with the measurements of Deardorff & Willis (1967). The presence of the mean shear in run 8 increases the horizontal velocity fluctuations substantially through the process of the energy transfer from the mean to the fluctuating velocity field.

Non-normalized one-dimensional velocity and temperature spectra (20) in the x -direction for run 7 are plotted in figure 16. The spectra decay by more than 3 orders of magnitude in the wavenumber range delimited by the spatial resolution and size of the computational domain. This is consistent with an adequately resolved simulation. The spectra show the presence of weak secondary maxima at $k \approx 4$, which corresponds to the wavelength $\lambda = 1.25$. The presence of the secondary maxima in the spectra at wavelengths $0.7 < \lambda < 1.7$ was reported by Deardorff & Willis (1967). In the numerical simulations of Grötzbach (1983), no secondary maxima were observed, and he argued that long time averaging of the data should always give continuous spectra without discrete peaks. However, instantaneous

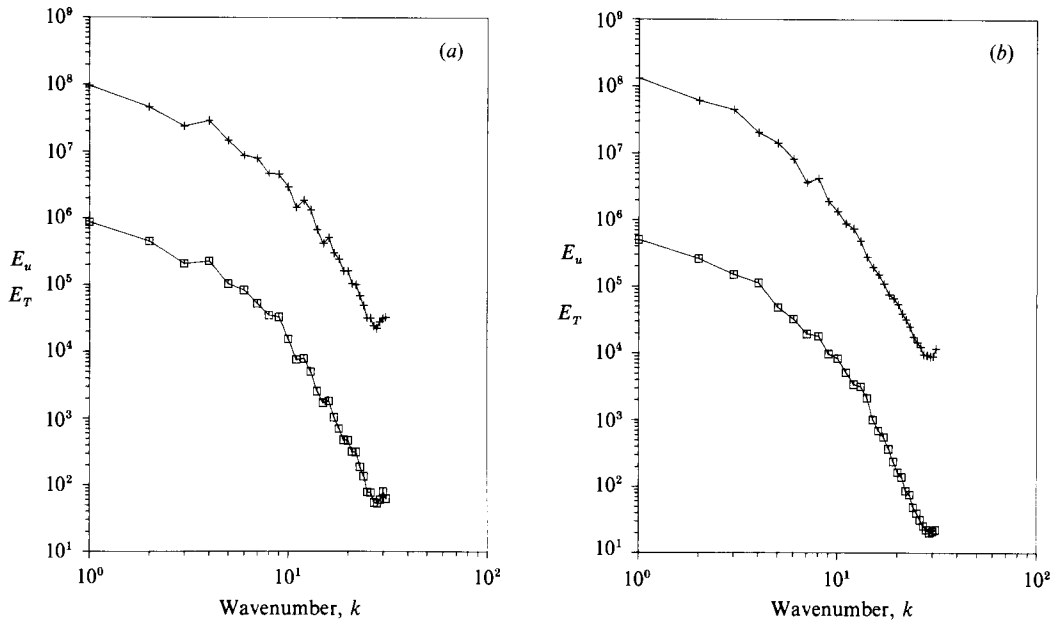


FIGURE 16. One-dimensional velocity and temperature spectra in the x -direction: \square , velocity; $+$, temperature: (a) Run 7. (b) Run 8.

spectra (or spectra averaged over short times as in experiments) may have discrete peaks due to the presence of slowly evolving spatial structures with these wavenumbers.

5.4. $Ra = 630\,000$

An attempt has been made to simulate turbulent convection at $Ra = 630\,000$, which corresponds to the lowest value of the Rayleigh number in the experiments of Deardorff & Willis (1967). Using the analysis of §4, it was determined that convection with $Ra = 630\,000$ and $Nu \approx 7$ could be adequately simulated with $64^2 \times 33$ modes if $L_x \approx L_y \approx 5$. In practice, however, we have found that the boundary layers were not resolved accurately enough, based on an analysis of the kinetic-energy and the temperature-variance equations. Despite this, the convective-core-results are in fairly good agreement with the experiments of Deardorff & Willis (1967) and, for this reason, we include a short discussion of some of our results obtained at $Ra = 630\,000$.

The Nusselt number for run 9, $Nu = 7.60$, is higher than $Nu \approx 6$ reported by Deardorff & Willis (1967), but this may be attributed to horizontal dimensions of the computational domain that were too small. The Nusselt number for the shear case drops to $Nu = 5.80$ (table 2) in agreement with the analysis of the results at $Ra = 150\,000$. Peak values of the instantaneous r.m.s. velocities for run 9 (figure 17*a*) are in good agreement with the experimental results. In the case with mean shear (run 10), horizontal components of the fluctuating velocity were no longer isotropic, as they were in run 8. The value of u_{rms} was consistently higher than the value of v_{rms} during the time of the simulation. At this higher Rayleigh number and lower relative shear ($Ri = -0.3$ versus $Ri = -0.2$ in run 7), the mixing action of the convection was not strong enough to equalize the horizontal velocities. Figure 17(*b*) shows the terms in the temperature-variance budget. Although the qualitative behaviour of these

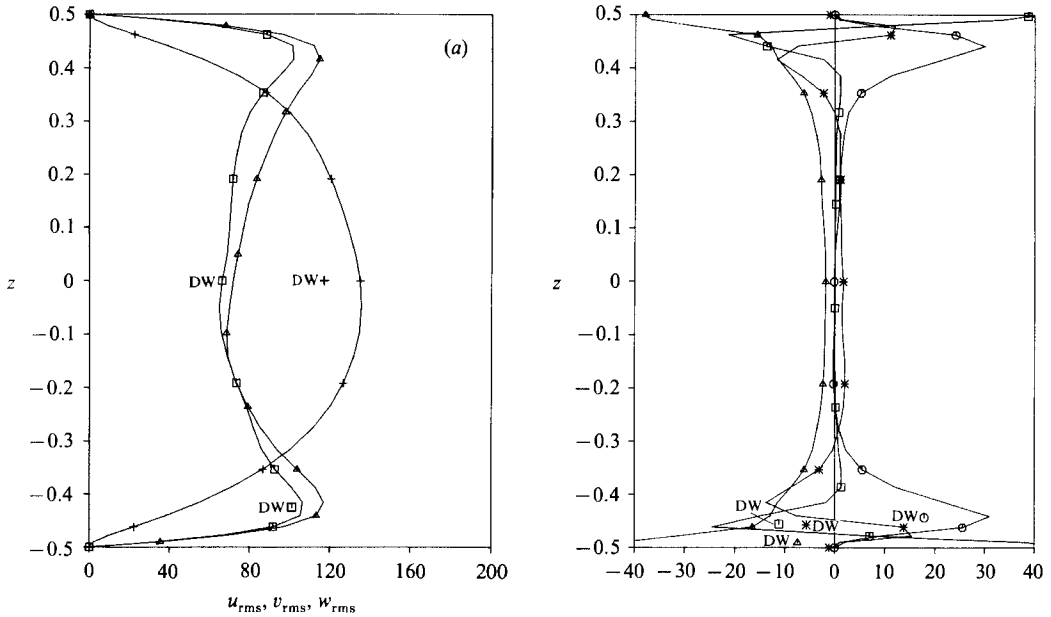


FIGURE 17. Run 9: $Ra = 630000$; $Ri = -\infty$; $t = 0.02$. (a) The vertical structure of the r.m.s. velocities. For a description of the symbols, see caption to figure 15. Points denoted DW represent experimental results of Deardorff & Willis (1967). (b) The vertical structure of the terms in the thermal-variance equation. For a description of the symbols, see caption to figure 14.

curves is the same as in the experiments (Deardorff & Willis 1967, figure 17), the absolute peak values of the individual terms in the boundary layers are substantially overestimated, with the accuracy deteriorating as the boundary is approached. It becomes apparent that the vertical resolution at the boundaries should be increased even though we already have five mesh points in the boundary layer $\delta_T \approx 1/(2Nu)$. The requirement to have at least three mesh points in the boundary layer δ_T in order to simulate turbulent convection accurately (Grötzbach 1983) seems to be too weak at high Rayleigh numbers. In the high-resolution simulations of Eidson *et al.* (1986), eight points in the thermal boundary layer were used to resolve it adequately (a total of 65 points in the vertical at $Ra = 380000$). Nevertheless, most of the gross features of the convection outside the boundary layers are reproduced adequately even with lower resolution. This is a reflection of the fact that the dynamics of the convective core are governed by the large-scale spatial structures, which are easily resolved even with a limited number of mesh points. This also explains an apparent success of subgrid-scale modelling of turbulent convection (Eidson 1985; Deardorff 1970), which is a way of accurately capturing the dynamics of the large scales and approximating the dynamics of the small scales.

6. Conclusions

In this paper we have reported results of direct numerical simulations of natural convection in plane Couette flow. To solve the equations of motion (5) we have employed an accurate numerical pseudospectral code. The highest resolution used in our simulations corresponds to 64^2 modes in the horizontal and 33 in the vertical. All simulated flows were at sufficiently high Rayleigh numbers to produce turbulent

convection ($Ra > 12000$). It was found that the main qualitative effect of shear is to organize large-scale convective structures in the direction of the mean velocity. The effect of shear on heat transfer depends on the Rayleigh number. For moderate Rayleigh numbers, $12000 \lesssim Ra \lesssim 50000$ (runs 1–6), the level of turbulence is small, and shear is capable of organizing the convective structures in the form of quasi-two-dimensional rolls. This can lead to a slightly higher heat transfer than for less organized convection without shear at the same Rayleigh number. At larger Rayleigh numbers ($Ra \gtrsim 150000$), shear cannot organize the convection into a two-dimensional state. In fact, at these higher Rayleigh numbers, shear seems to decrease the level of organization of the convective structures by tearing off and disrupting plumes transferring heat between the plates. This effectively decreases the heat transfer in shear run 8.

The unsteadiness of the convection is reflected in the complex time dependence of the velocity and temperature fields as well as global quantities such as the Nusselt number. The oscillatory time behaviour of the Nusselt number is caused by the action of the convective thermals pumping hot fluid toward the upper plate and the inertial effects returning some of this fluid back down towards the lower plate. This last process slows the convective rolls until increased heat transfer at the lower boundary speeds them up again.

An analysis of the energy-balance equation indicates that most of the energy production due to buoyancy effects occurs in a relatively uniform convective core and the energy production due to shear effects is concentrated in the boundary layers. It was found that among diffusive terms, the pressure-diffusion term was quite important in redistributing kinetic energy inside the convective layer, contrary to the assumptions made in some turbulence models.

The apparent connection between the level of organization of the convection and the heat transfer seen in our simulations suggests that it may be possible to increase heat transfer at a given Rayleigh number by manipulating or forcing the large-scale convective structures. Some possible ways of achieving this goal are the subject of ongoing investigation by the present authors.

This work was supported by the Department of Energy under Contract No. DE-AC06-84ER13153. Some computer time was provided by NAS at the NASA Ames Research Center.

REFERENCES

- AHLERS, G. & BEHRINGER, R. P. 1978 Evolution of turbulence from the Rayleigh–Bénard instability. *Phys. Rev. Lett.* **40**, 712–716.
- BERGÉ, P. & DUBOIS, M. 1976 Time dependent velocity in Rayleigh–Bénard convection: a transition to turbulence. *Optics Commun.* **19**, 129–133.
- BROWN, W. 1973 Heat-flux transitions at low Rayleigh number. *J. Fluid Mech.* **60**, 539–559.
- BUSSE, F. H. 1972 The oscillatory instability of convection rolls in a low Prandtl number fluid. *J. Fluid Mech.* **52**, 97–112.
- CHANDRASEKHAR, S. 1961 *Hydrodynamic and Hydromagnetic Stability*. Clarendon.
- CHU, T. Y. & GOLDSTEIN, R. J. 1973 Turbulent convection in a horizontal layer of water. *J. Fluid Mech.* **60**, 141–159.
- CLEVER, R. M. & BUSSE, F. H. 1974 Transition to time-dependent convection. *J. Fluid Mech.* **65**, 625–645.
- CLEVER, R. M. & BUSSE, F. H. 1977 Instabilities of longitudinal convection rolls in an inclined layer. *J. Fluid Mech.* **81**, 107–127.

- CLEVER, R. M., BUSSE, F. H. & KELLY, R. E. 1977 Instabilities of longitudinal convection rolls in Couette flow. *Z. angew. Math. Phys.* **28**, 771–783.
- CONSTANTIN, P., FOIAS, C., MANLEY, O. P. & TEMAN, R. 1985 Determining modes and fractal dimension of turbulent flows. *J. Fluid Mech.* **150**, 427–440.
- CURRY, J. H., HERRING, J. R., LONCARIC, J. & ORSZAG, S. A. 1984 Order and disorder in two- and three-dimensional Bénard convection. *J. Fluid Mech.* **147**, 1–38.
- DALY, B. J. 1974 A numerical study of turbulence transitions in convective flow. *J. Fluid Mech.* **64**, 129–165.
- DEARDORFF, J. W. 1970 A numerical study of three-dimensional turbulent channel flow at large Reynolds numbers. *J. Fluid Mech.* **41**, 453–480.
- DEARDORFF, J. W. 1973 Three-dimensional modeling of the planetary boundary layer. In *Workshop in Micrometeorology* (ed. D. A. Haugen), p. 271. American Meteorology Society.
- DEARDORFF, J. W. & WILLIS, G. E. 1967 Investigation of turbulent thermal convection between horizontal plates. *J. Fluid Mech.* **28**, 675–704.
- DEARDORFF, J. W. & WILLIS, G. E. 1985 Further results from a laboratory model of the convective planetary boundary layer. *Boundary-Layer Met.* **32**, 205–236.
- DUBOIS, M. & BERGÉ, P. 1978 Experimental study of the velocity field in Rayleigh–Bénard convection. *J. Fluid Mech.* **85**, 641–653.
- EIDSON, T. M. 1985 Numerical simulation of the turbulent Rayleigh–Bénard problem using subgrid modelling. *J. Fluid Mech.* **158**, 245–268.
- EIDSON, T. M., HUSSAINI, M. Y. & ZANG, T. A. 1986 Simulation of the turbulent Rayleigh–Bénard problem using a spectral/finite difference technique. *ICASE Rep.* 86-6.
- GOLDSTEIN, R. J. & CHU, T. Y. 1969 Thermal convection in a horizontal layer of air. *Prog. Heat Mass Transfer* **2**, 55.
- GOLLUB, J. P., HULBERT, S. L., DOLNY, G. M. & SWINNEY, H. L. 1977 In *Proton Correlation Spectroscopy* (ed. F. Cummins & E. R. Pike). Plenum.
- GOTTLIEB, D., HUSSAINI, M. Y. & ORSZAG, S. A. 1984 Theory and application of spectral methods. In *Spectral Methods for Partial Differential Equations* (ed. R. G. Voigt, D. Gottlieb & M. Y. Hussaini), pp. 1–54. SIAM.
- GRÖTZBACH, G. 1982 Direct numerical simulation of laminar and turbulent Bénard convection. *J. Fluid Mech.* **119**, 27–53.
- GRÖTZBACH, G. 1983 Spatial resolution for direct numerical simulation of the Rayleigh–Bénard convection. *J. Comp. Phys.* **49**, 241–264.
- HART, J. E. 1971 Stability of the flow in a differentially heated inclined box. *J. Fluid Mech.* **47**, 547–576.
- HATHAWAY, D. A. & SOMERVILLE, R. C. J. 1986 Nonlinear interactions between convection, rotation and flows with vertical shear. *J. Fluid Mech.* **164**, 91–105.
- HINZE, J. O. 1975 *Turbulence*. McGraw-Hill.
- HOWARD, L. N. 1964 Convection at high Rayleigh numbers. In *Proc. Eleventh Intl Congr. Applied Mechanics, München* (ed. Görtler, H.), pp. 1109–1115. Springer.
- INGERSOLL, A. P. 1966 Thermal convection with shear at high Rayleigh number. *J. Fluid Mech.* **25**, 209–228.
- KRISHNAMURTI, R. 1970*a* On the transition to turbulent convection. Part 1. The transition from two- to three-dimensional flow. *J. Fluid Mech.* **42**, 295–307.
- KRISHNAMURTI, R. 1970*b* On the transition to turbulent convection. Part 2. The transition to time-dependent flow. *J. Fluid Mech.* **42**, 309–320.
- KRISHNAMURTI, R. 1973 Some further studies on the transition to turbulent convection. *J. Fluid Mech.* **60**, 285–303.
- KUO, H. L. 1963 Perturbations of plane Couette flow in stratified fluid and origin of cloud streets. *Phys. Fluids* **6**, 195–211.
- LIPPS, F. B. 1971 Two-dimensional numerical experiments in thermal convection with vertical shear. *J. Atmos. Sci.* **28**, 3–19.
- LIPPS, F. B. 1976 Numerical simulation of three-dimensional Bénard convection in air. *J. Fluid Mech.* **75**, 113–148.

- LIPPS, F. B. & SOMERVILLE, R. C. J. 1971 Dynamics of variable wavelength in finite-amplitude Bénard convection. *Phys. Fluids* **14**, 759-765.
- MALKUS, W. V. R. 1954 Discrete transitions in turbulent convection. *Proc. R. Soc. Lond. A* **225**, 196-212.
- MANLEY, O. P. & TREVE, Y. M. 1981 Minimum number of modes in approximate solutions to equations of hydrodynamics. *Phys. Lett.* **82A**, 88-90.
- MARCUS, P. S. 1984 Simulation of Taylor-Couette flow. Part 1. Numerical methods and comparison with experiment. *J. Fluid Mech.* **146**, 45-64.
- MCLAUGHLIN, J. B. & ORSZAG, S. A. 1982 Transition from periodic to chaotic thermal convection. *J. Fluid Mech.* **122**, 123-142.
- MELLOR, G. L. & YAMADA, T. 1982 Development of a turbulence closure model for geophysical fluid problems. *Rev. Geophys. Space Phys.* **20**, 851-875.
- MONIN, A. S. & YAGLOM, A. M. 1979 *Statistical Fluid Mechanics*, Vol. 1. MIT Press.
- ORSZAG, S. A. & KELLS, L. C. 1980 Transition to turbulence in plane Poiseuille and plane Couette flow. *J. Fluid Mech.* **96**, 159-205.
- RICHTER, F. M. & PARSONS, B. 1975 On the interaction of two scales of convection in the mantle. *J. Geophys. Res.* **80**, 2529-2541.
- ROSSBY, T. 1969 A study of Bénard convection with and without rotation. *J. Fluid Mech.* **36**, 309-335.
- SCHLÜTER, A., LORTZ, D. & BUSSE, F. 1965 On the stability of steady finite amplitude convection. *J. Fluid Mech.* **44**, 661-672.
- SPARROW, E. M. & HUSAR, R. B. 1969 Longitudinal vortices in natural convection flow on inclined plates. *J. Fluid Mech.* **37**, 251-255.
- THRELFALL, D. C. 1975 Free convection in low-temperature gaseous helium. *J. Fluid Mech.* **67**, 17-28.
- TOWNSEND, A. A. 1959 Temperature fluctuations over a heated horizontal surface. *J. Fluid Mech.* **5**, 209-241.
- TURNER, J. S. 1973 *Buoyancy Effects in Fluids*. Cambridge University Press.
- VERONIS, G. 1966 Large amplitude Bénard convection. *J. Fluid Mech.* **26**, 49-68.
- WILLIS, G. E. & DEARDORFF, J. W. 1965 Measurements on the development of thermal turbulence in air between horizontal plates. *Phys. Fluids* **8**, 2225.
- WILLIS, G. E. & DEARDORFF, J. W. 1970 The oscillatory motions of Rayleigh convection. *J. Fluid Mech.* **44**, 661-672.
- WILLIS, G. E., DEARDORFF, J. W. & SOMERVILLE, R. C. J. 1972 Roll-diameter dependence in Rayleigh convection and its effect upon heat flux. *J. Fluid Mech.* **54**, 351-367.